A Numerical Study of the Genesis of Tropical Storms Observed during the FGGE Year

ROBERT E. TULEYA

Geophysical Fluid Dynamics Laboratory/NOAA, Princeton, New Jersey

(Manuscript received 3 September 1987, in final form 14 December 1987)

ABSTRACT

This study utilizes the First GARP Global Experiment's (FGGE) analyzed dataset and a relatively fine scale regional model in combination to investigate the feasibility of numerically simulating tropical disturbances during the FGGE year, 1979. Four different cases were investigated including a cyclone, TC-17, in the Indian Ocean, a developing hurricane, David, and a nondeveloping wave in the Atlantic, and a multi-storm case, Tip and Roger, in the Pacific.

The results were promising when using ECMWF FGGE data in that simulations of genesis or nongenesis were achieved in the three developing cases and in the one nondeveloping case. The accuracy of the intensification rates varied from case to case. For example, in the simulation of TC-17, the maximum low level winds were simulated to be ~45 m s^{-1} while observations indicated winds of only 22 m s^{-1}. However, in the case of David, the maximum winds increased at a slower rate than observed, while in the case of Tip the slow intensification rate was correctly simulated. An interesting result was the high correlation between model precipitation patterns in the simulations and observed satellite cloud photos. These results indicate that the environment in which an incipient disturbance is embedded plays a major role in the genesis process. An additional striking result was the wide variability of storm development and structure from case to case. Tropical storm David was simulated to be a relatively small scale storm whereas Tip was simulated to be a storm with an enormous area of gale force winds. The model simulations also produced different distributions of the low level wind maximum relative to the moving storm with banding of a number of meteorological fields, including precipitation and vorticity. The formation of storms was related to the presence of an incipient disturbance possessing cyclonic low level vorticity, and ample high relative humidity together with a strong coupling between the disturbance phase speed and the upper level flow field. Most cases including the nondeveloping wave contained upper level anticyclonic conditions. All cases included a weak warm, upper level anomaly including the nondeveloping wave case. Also, it was found that environmental upward motion is not always an accurate indicator of genesis.

1. Introduction

The tropical cyclone is an integral part of the weather activity in most tropical ocean basins and its influence extends into the extratropics as well. The evolution of the phenomena has created interest for decades. The life cycle of tropical cyclones has been categorized into stages beginning from an early incipient stage of a cloud cluster or easterly wave, and extending to a depression, to a tropical storm, to a hurricane or typhoon stage, and finally to a decay or extratropical transformation stage. Historically genesis of a tropical storm is defined as the attainment of low level sustained gale force (~17 m s^{-1}) winds by a tropical system. This definition will be used in this study. To date, operational forecasts have concentrated on the important question of track of preexisting, mature tropical cyclones. The forecast and understanding of the genesis phenomena has been left for research studies. Theoretical studies on genesis have emphasized distinct mechanisms responsible for intensification. These mechanisms include the concepts of CISK (Charney and Eliassen 1964; Ooyama 1964), nonlinear advection of vorticity (Shapiro 1977), nonlinear response due to specified heating (Hack and Schubert 1986), and air-sea interaction of a finite amplitude disturbance (Rotunno and Emanuel 1987). Observational investigations include case studies by Yanai (1961a, 1961b, 1968), Hebert (1978), and Sadler (1978), the classic climatological study by Gray (1968), and composite studies (e.g., McBride and Zehr 1981). All these studies have contributed to our knowledge of tropical cyclone genesis, although none by itself has unveiled what can be considered the primary mechanism of genesis. Genesis is a complex phenomenon with no single, distinct instability mechanism and with a wide variability in the evolution of tropical storms. This includes a variability in the basic state of each formation basin and the wide variability in frequency of occurrence from season to season and from week to week.

Modeling studies of observed genesis have been confined to early attempts by Miller et al. (1972) and Ceselski (1974) to predict wave amplification and predictions of tropical waves and monsoon depressions by Krishnamurti et al. (1983, 1984). Interestingly,

Corresponding author address: Robert E. Tuleya, NOAA/ERL/GFDL, Princeton University, P.O. Box 308, Princeton, NJ 08542.

global models contain the development of hurricane-like features in the tropics (Manabe 1970) with their results becoming more realistic (Bengtsson 1982; Digon 1987). It remains to be seen with what degree of accuracy these models can forecast genesis and what model resolution and observation density are needed. On the other hand, more sophisticated, realistic simulations have been performed for the genesis stage in which the influences of a variety of idealized basic environmental flows were investigated (Tuleya and Kurihara 1981).

The FGGE year provides an excellent opportunity to study tropical cyclone activity from the global perspective. Some results of studies using the FGGE dataset involving tropical cyclones (e.g., Lee 1986) have been encouraging in that both incipient and mature storms could be followed and analyzed despite the rather coarse resolution and inadequate observational data. The FGGE year generally brought less than average tropical cyclone activity in the Western North Pacific and the Atlantic, and above average tropical cyclone activity in the North Indian Ocean. In the Western Pacific, there were 23 tropical cyclones compared to a long term-average of 28. In the Atlantic, there were 8 storms compared to an average of 10 (five landfalls were observed). The post-monsoon period in the Indian Ocean was quite active with six storms. For the entire year, a total of seven storms occurred compared to a climatological average of four.

The primary purpose of this study is to investigate the feasibility of combining a high resolution, sophisticated regional model with a realistic dataset, to simulate genesis. Several cases in the FGGE year will be used. The storm's tracks and intensification rates in the model will then be compared to observation. Using the simulated results, some finer details will be investigated such as the storm structure, warm core formation, and the diversity of evolution from one case to another. This diversity is hard to study with idealized initial conditions.

The assumption made in this study is that the analyzed initial large scale fields and physics of the present model are, at least, adequate for studying the genesis phenomena. This approach does not attempt to answer the question of the formation of an initial disturbance, but assumes that a cloud cluster, a tropical wave, or some finite amplitude disturbance exists prior to genesis. The evolution of tropical disturbances involve a wide range of scales including the cloud scale up through planetary scales. Implicit in this study is the belief that at some stage prior to achieving tropical storm strength, an incipient storm's evolution is influenced to a large extent by the relatively large scale environmental conditions.

In section 2, the datasets utilized and their subsequent implementation in the experimental design of this study will be discussed. Numerical experiments on four distinct case studies will be described in section 3 with emphasis on the initial conditions and basic features of storm track and intensification rate. Section 4 contains more detailed information on the experiments described in section 3 including precipitation patterns, storm size, and storm genesis criteria. Section 5 contains the summary and conclusions. Some assessment of the predictive skill of the regional model system of this study will be briefly discussed in the Appendix by analyzing the sensitivity of the results to both initial and lateral boundary conditions.

2. Analysis of FGGE IIIB and experimental design

a. Use of FGGE-IIIB as the primary dataset

During 1979, an extensive, worldwide effort was made to collect, analyze, and archive atmospheric data for scientific study. This experiment was termed FGGE (First Garp Global Experiment) and the objectively analyzed data for the entire globe is referred to as FGGE IIIB. Two centers have analyzed the whole year, GFDL (Geophysical Fluid Dynamics Laboratory) and ECMWF (European Centre for Medium Range Weather Forecasting). The resolution for this archived data is 1.875 degree longitude by 1.875 degree latitude. This resolution was shown by Miyakoda et al. (1980) to be capable of resolving easterly waves and incipient disturbances for the Garp Atlantic Tropical Experiment period. Of course the accuracy of the structure of the disturbances as analyzed in FGGE IIIB is dependent on the available data input, the analysis technique, and the numerical model used in the analysis. It can be shown that the accuracy of hurricane scale ($\sim$200 km) motions is handicapped by both data availability and analysis grid resolution. However, the basic assumption is that the global FGGE IIIB analysis can, to a reasonable extent, resolve the essential environmental features for development of a tropical storm. Specifically, incipient tropical disturbances exist prior to storm development and they appear more or less realistically analyzed in FGGE IIIB.

b. Other data sources

The FGGE IIIB data analyses used climatological sea surface temperature (SST). It has been shown that accurate values of SST may be needed for studies and prediction of tropical cyclone evolution (e.g., Wendland 1977; Shapiro 1982; Chang and Madala 1980; Tuleya and Kurihara 1982). Therefore monthly mean values of SST were obtained from the Climate Analysis Center (CAC) for the FGGE year.

For verification purposes, track and intensity of storms are obtained from the National Hurricane Center (NHC, Miami) and the Joint Typhoon Warning Center (JTWC, Guam). Generally this best track data, obtained from reconnaissance aircraft and satellite interpretation, is available at six hour intervals beginning from a first fix position a day or so before development

into a tropical storm. Satellite photos were also used to compare precipitation areas simulated with the model to disturbed cloud areas. Also available are the NHC and JTWC operational forecasts. Forecasts of track and intensity are generally initiated at the depression stage and often a day or so prior to storm development.

c. Analyses of data onto model domain

The data were obtained from the different sources, and interpolated horizontally using various methods onto the regional model domain. For the u and v wind components, a fourth-order polynomial fit described by Akima (1978) was used. This technique gave a smooth fit of not only the wind components, but also the first derivative quantities of the momentum such as vorticity and divergence. Otherwise for all fields requiring horizontal interpolation a simple bilinear interpolation was used. Vertical interpolation was performed next after the fields were horizontally interpolated. A cubic spline technique utilized by GFDL FGGE IIIB data archival (Ploshay et al. 1983) was used to interpolate values from the archived pressure levels to the model sigma levels given the specified topographical heights and the derived surface pressure. As recommended by the ECMWF (Bjorheim et al. 1981), the temperature fields were calculated hydrostatically from the given geopotential height and relative humidity fields.

d. Model description

The regional model used is nearly identical to that used in the studies of Kurihara and Tuleya (1981) and Tuleya and Kurihara (1981). It is a uniform resolution version of that used by Kurihara and Bender (1980) except for the inclusion of radiation parameterization. The model includes cumulus parameterization by Kurihara (1973), level-two turbulent closure in the vertical (Mellor and Yamada 1974), a Monin-Obukov constant surface layer and a nonlinear horizontal diffusion (Smagorinsky 1963). The radiation package is a simplified version of that by Wetherald and Manabe (1980) except a simple cloud specification scheme is implemented (i.e., clouds are assumed to exist where model condensation occurs). The grid resolution is uniform 0.25 deg in longitude and latitude and the vertical resolution has eleven layers, ranging from $\sigma = 0.0306$ (k level = 1) to $\sigma = 0.992$ (k level = 11), with three in the planetary boundary layer. The domain is specified as 36° longitude by 30° latitude and can be moved to the specified area of interest. The horizontal grid resolution was chosen to be fine enough to resolve hurricane force winds readily. The domain was chosen to enable a storm to move through its development cycle with boundaries having little detrimental effect. The domain size was also chosen large enough for multiple storm cases. The impact of domain size and boundary conditions will be discussed in some detail in the Appendix.

The model lateral boundary scheme used is that proposed by Kurihara and Bender (1983). This boundary condition initially approximates boundary fluxes by extrapolation of momentum and moisture to the boundary combined with a corresponding geostrophic and thermal wind balance to obtain the temperature and surface pressure. The normal wind component and the tangential wind component at inflow are then forced toward a specified value. This leads to the regional model being run in two distinct modes. When the specified values are derived from a larger domain model forecast, the mode is defined as a *forecast*, while the mode is defined as a *simulation* when the lateral boundary is specified from an observational analysis (Orlanski 1987). In the simulation mode, the boundary values are taken every 12 h from the FGGE IIIB dataset, the same dataset that is used to define the initial atmospheric conditions. In the forecast mode, the boundary values are obtained from the R30L18 Spectral Model of GFDL (Gordon and Stern 1982); this model has rhomboidal spectral truncation at wavenumber 30 in the horizontal and 18 sigma levels in the vertical and is nearly identical to that used for the GFDL FGGE IIIB analysis (see Ploshay et al. 1983 for a more detailed description). In either case the specified values are linearly interpolated in time to hourly values. The model solution is then forced toward these updated, hourly values every time step.

e. Experimental design

For this study cases were selected so that the initial condition was at least one day prior to genesis (i.e., to be pre-storm with maximum surface winds < 17 m s^{-1}) as estimated by best track information. Often best track data was not available for the initial storm location. For each case the domain was positioned to contain relevant features such as the initial disturbance and the environment in which it interacts. The model was integrated three days covering the development or non-development period. The initial condition was taken by the analysis method described in section 2a–c. No further initialization was attempted. It was hoped that the initial fields were in approximate dynamic balance since they were obtained from data assimilated by a dynamic model. It is recognized that this assumption might depend on the phenomenological scale of interest and both the assimilating model as well as the regional model being used. Nevertheless this question is left for further research.

For this study three developing and one nondeveloping cases were investigated. In order to test a variety of conditions, cases were studied in three different geographical domains. Table 1 includes a list of the experiments performed for this investigation. The cases include one in the Indian Ocean in May, developing

TABLE 1. The list of experiments performed.

Experiment	Initial condition	Model	Domain	Lateral boundary condition
		5–8 May		
M05	ECMWF	Regional	10°S–20°N, 64°–100°E	FGGE ANAL
M05G	GFDL	Regional	10°S–20°N, 64°–100°E	FGGE ANAL
M05F	ECMWF	Regional	10°S–20°N, 64°–100°E	R30L18 FCST
M05S	ECMWF	R30L18SPEC	Global	—
		18–21 Aug.		
A18	ECMWF	Regional	3°S–27°N, 60°–24°W	FGGE ANAL
A18G	GFDL	Regional	3°S–27°N, 60°–24°W	FGGE ANAL
A18F	ECMWF	Regional	3°S–27°N, 60°–24°W	R30L18 FCST
A18S	ECMWF	R30L18SPEC	Global	—
		25–28 Aug.		
A25	ECMWF	Regional	3°S–27°N, 60°–24°W	FGGE ANAL
A25G	GFDL	Regional	3°S–27°N, 60°–24°W	FGGE ANAL
A25F	ECMWF	Regional	3°S–27°N, 60°–24°W	R30L18 FCST
A25S	ECMWF	R30L18SPEC	Global	—
		4–7 Oct.		
O04	ECMWF	Regional	3°S–27°N, 126°–162°E	FGGE ANAL
O04G	GFDL	Regional	3°S–27°N, 126°–162°E	FGGE ANAL
O04F	ECMWF	Regional	3°S–27°N, 126°–162°E	R30L18 FCST
O04S	ECMWF	R30L18SPEC	Global	—

and non-developing cases in the Atlantic in August, and a developing case in the Western Pacific in October. For this study, more emphasis will be put on the regional model experiments performed in simulation mode with ECMWF FGGE IIIB used as initial conditions since the GFDL FGGE IIIB has some shortcomings (Stern et al. 1985). The results of simulation Exps. M05, A18, A25 and O04 will be presented in sections 3 and 4. Results of the regional model in forecast mode, spectral forecasts, and experiments with GFDL FGGE IIIB as initial conditions will be discussed in the Appendix.

3. Simulation of developing and nondeveloping disturbances

As was mentioned, four distinct cases were investigated. The details of these cases will be discussed for the simulation mode utilizing the ECMWF FGGE IIIB dataset in this and the next section. In this section the initial conditions as well as the gross time evolution of the major features such as maximum wind and surface pressure fields will be presented.

a. Tropical cyclone in the Indian Ocean in May

The first case to be discussed is that of a tropical cyclone, TC-17, in the Indian Ocean. This was the strongest cyclone during the FGGE year for the Indian Ocean basin and made landfall on the eastern coast of India on 12 May. The initial sea level pressure analysis is shown for the computational domain at 00Z 5 May in Fig. 1. Also shaded is the low level vorticity greater than 10×10^{-6} s^{-1}. The low level analysis indicates a monsoon trough extending from the southern coast of India southeastward into the Indian Ocean with a weak but well defined low level circulation centered near 8°N, 91°E (Fig. 2). Other significant features include a southern hemisphere storm and an area of high low level westerly winds located on the equator extending from 80° to 90°E. Aloft there existed an anticyclone to the northeast over Bangladesh at ~335 mb (k = 4) extending over the Bay of Bengal at ~215 mb (k = 3). Easterly vertical wind shear therefore extended from the surface to the tropopause. The circularly-averaged disturbance structure can be seen in Fig. 3. Positive vorticity extends to ~335 mb although values larger than 20×10^{-6} are confined to the lower half of the atmosphere and to within 3.5 degrees from the center. A warm anomaly relative to the outer area is weak (~0.2 K) and is confined to middle levels. High relative humidities exist at low levels near the storm center.

In Exp. M05 the initial perturbation drifted slowly southwestward for the first day. During this time convective activity increased as a warm core developed aloft over the low level disturbance. Interestingly, subsidence surrounded the convective area, which caused the 15° × 15° storm area average vertical motion to be downward (~3 mb h^{-1} at 500 mb at 12 h after the initial time). The disturbance then moved west, then northwest and intensified into a tropical storm with minimum pressure of 967 mb at 72 h at the end of the simulation. Figure 4 indicates the sea level pressure field valid at 00Z 8 May together with the positions every 24 h of Exp. M05 and the observed best track. Although there is no best track fix location for the initial

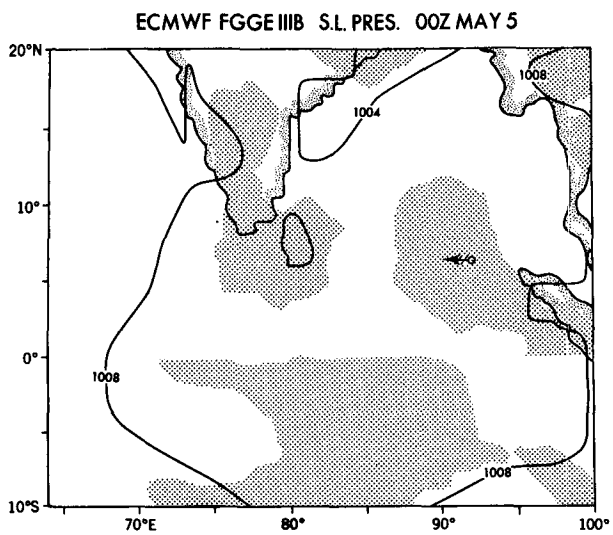

FIG. 1. The sea level pressure analysis of the ECMWF FGGE IIIB dataset for 00Z 5 May 1979 for the regional domain of Exp. M05. Shading indicates cyclonic vorticity greater than 10×10^{-6} s^{-1} at ~950 mb (k = 9). The arrow indicates the first reported best track fix of TC-17 by JTWC at 08Z 5 May and its track is extrapolated back to the 00Z 5 May position indicated by the open circle.

time there appears to be a position difference between the extrapolated best track and the initial analysis of about 250 km. This difference does not increase, but rather decreases to 129 and 91 km at 24 h and 48 h respectively. The model simulation, however, failed to turn to the southwest as TC-17 executed a tight loop on 8 May before proceeding northwest. Despite this, the difference between the best track and simulation was only 328 km at 72 h. The intensity of Exp. M05 can be compared to the best track information (Fig. 5). Experiment M05 overpredicted the intensity with low level winds exceeding 40 m s^{-1} at 72 h while JTWC best track information had winds of 22 m s^{-1}. It is interesting that the upper level outflow became associated with the southern hemispheric storm at about 00Z 6 May when the storm intensified. The maximum surface winds of the storm formed as an extension of the low level strong wind area near the equator southwest of the developing storm.

b. A nondeveloping wave in the Atlantic in August

The second case considered is that of a nondeveloping wave in the tropical Atlantic from 18 to 21 August (see Frank and Clark 1980). This wave did not intensify until 29 August when it developed into Tropical Storm Elena in the western Gulf of Mexico. The sea level pressure analysis for 00Z 18 August is shown in Fig. 6 together with cyclonic low level vorticity. There was a rather strong cyclonic disturbance associated with the cyclonic vorticity region centered near 12°N, 34°W (Fig. 7). Over this disturbed region, strong southwesterlies occurred at ~215 mb (k = 3). At ~335 mb (k = 4), there was an anticyclone to the east of the surface disturbance with westerlies to the northwest, while at ~120 mb (k = 2), a strong easterly jet extended from Africa. Cyclonic vorticity was confined to the lower troposphere with anticyclonic flow aloft as can be seen in a circular average around the disturbance center (Fig. 8). Strong low level surface convergence existed near the center of the disturbance. A weak warm anomaly existed at middle levels and increased near the surface to values exceeding 2 K. Values of relative humidity were relatively low, only exceeding 80% beyond 4° from the center. Low level winds exceeded 11 m s^{-1} to the north of this center.

In Exp. A18 considerable convective activity developed near the initial center and also with the equatorial trough to the south. The large scale tropical wave in

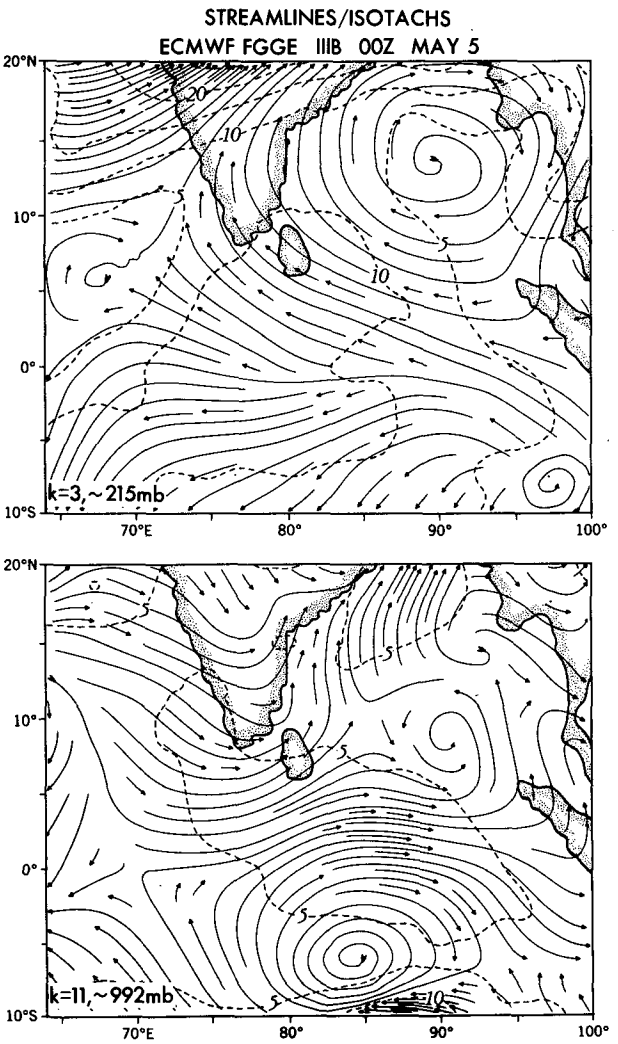

FIG. 2. Streamline and isotach analysis of the ECMWF FGGE IIIB dataset for 00Z 5 May 1979 for the regional domain of Exp. M05 (~215 mb, k = 3, upper; ~992 mb, k = 11, lower). Values of wind speed in m s^{-1}.

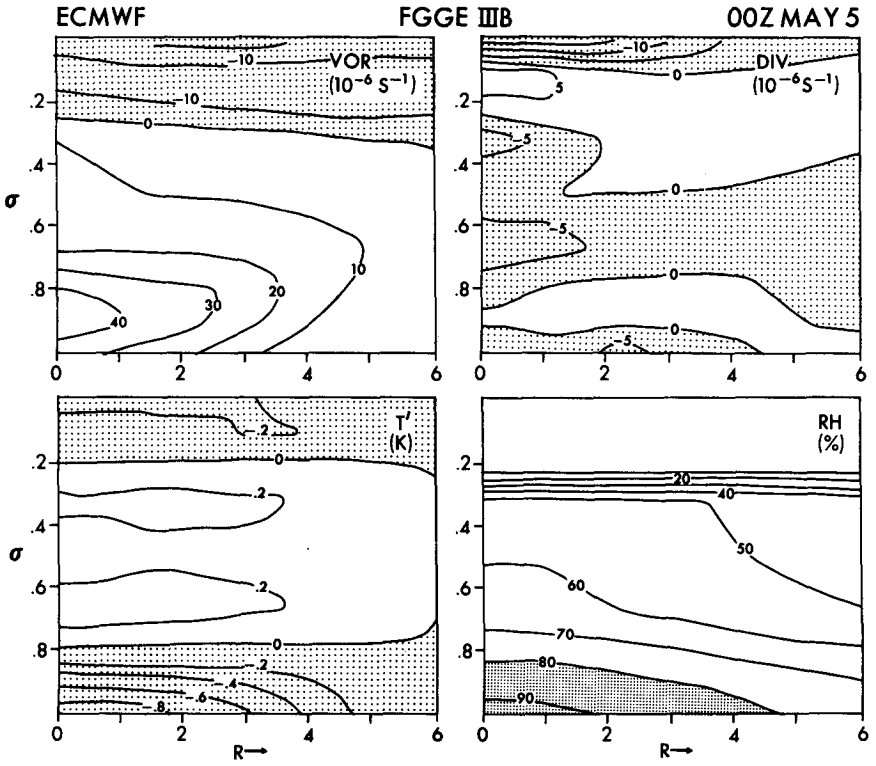

FIG. 3. Circular average cross sections of relative vorticity, divergence, temperature anomaly, and relative humidity for ECMWF FGGE IIIB for 00Z 5 May. The origin (6.2°N, 91.6°E) is taken from the disturbance center determined from the ECMWF data. The distance from the center is given in degrees latitude with each integer value being equivalent to approximately 111 km. The temperature anomaly is that relative to the mean temperature at 6 degrees radius from the center.

which the disturbance was embedded propagated to the west and was approximately at 10°N, 52°W at 00Z 21 August. This position corresponded quite well with the trough of the ECMWF FGGE IIIB analysis (Fig. 9, dashed line) and with the reported wave passage at Barbados by Frank and Clark (1980) on 22 August.

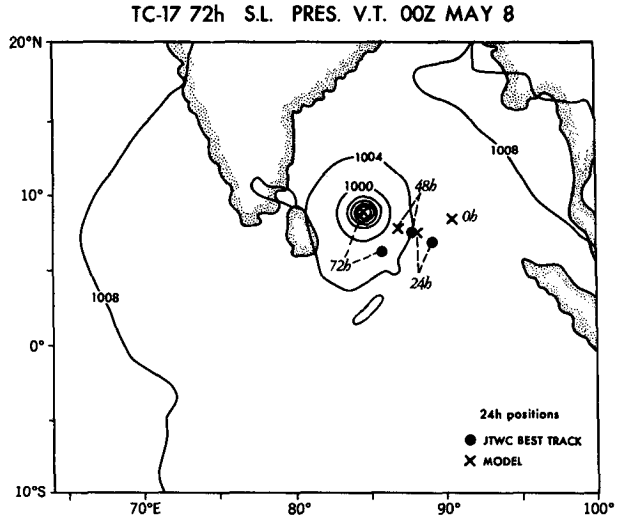

FIG. 4. The sea level pressure distribution of Exp. M05 for the verification time 00Z 8 May 1979. Daily storm positions of JTWC observations and model are given by dots and X's respectively.

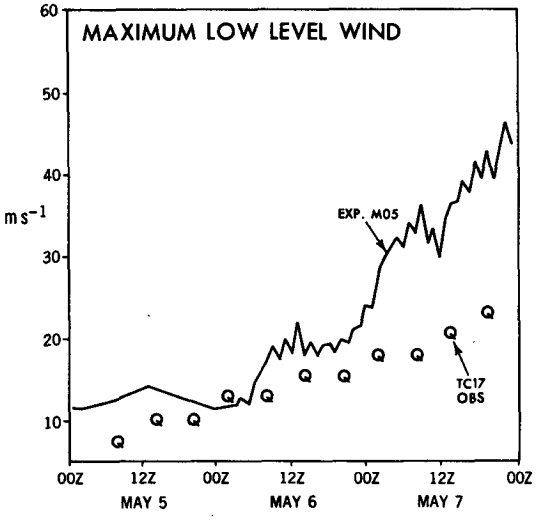

FIG. 5. The maximum low level wind at ~992 mb (k = 11) for Exp. M05 as a function of time. The JTWC observations of TC-17 are given by the letter "Q".

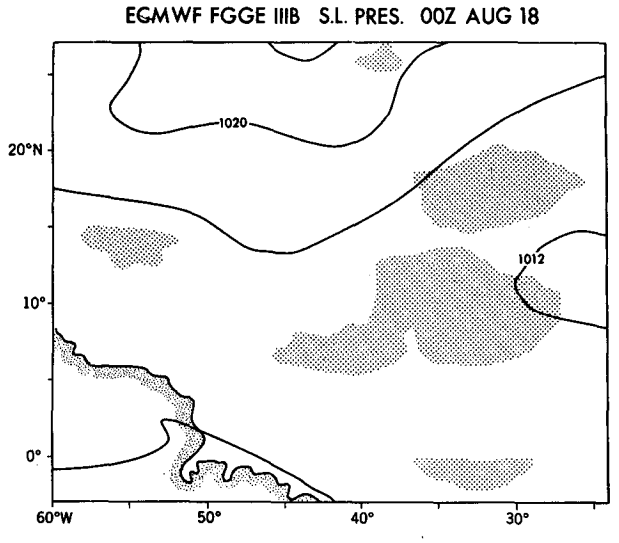

FIG. 6. The sea level pressure analysis of the ECMWF FGGE IIIB dataset for 00Z 18 Aug 1979 for the regional domain of Exp. A18. Shading indicates cyclonic vorticity greater than 10×10^{-6} s^{-1} at ~950 mb ($k = 9$).

After 00Z 19 August, the precipitation associated with the disturbance in Exp. A18 noticeably decayed. Through the first day or two the precipitation patterns simulated by the model corresponded quite well with the cloud photos in this region. This will be shown later in this study. The low level winds of Exp. A18 did not increase significantly during the three day simulation (Fig. 10, dashed line).

c. *The development of Hurricane David*

The third case simulated was that of Hurricane David from 00Z 25 August to 00Z 28 August. This storm later developed into a Category 5 hurricane which devastated the Leeward islands and Hispaniola. The initial sea level pressure field is shown in Fig. 11. A trough exists at 32°W with an associated cyclonic low level vorticity field. The low level wind pattern was quite similar to that of the nondeveloping case with cyclonic flow associated with the vorticity area and maximum winds 500 km to the northwest (Fig. 12). As in the nondeveloping case, a broad high pressure area was located to the north extending from the subtropics. In this case, however, westerlies were absent above the low level cyclonic area and the disturbance was therefore embedded in deep easterlies. The disturbance structure, itself, was quite different from the 18–21 August case as can be seen from Fig. 13. The initial system extended to the upper tropopause with relative vorticity values of 20×10^{-6} s^{-1} extending to 300 mb aloft and 4° from the center. The divergence pattern indicates a two node structure with surface convergence and 200 and 800 mb divergence. A weak warm anomaly occurred aloft centered at 400 mb. Another difference from the 18 August case was the relative moist conditions found on 25 August near the disturbance center in the lower troposphere.

In Exp. A25, the initial wave amplified and developed into a tropical storm. The wind maximum and upper level warm area to the northwest gradually became vertically aligned with the low level disturbance as it propagated westward at approximately 8 m s^{-1}. Associated with the low level disturbance was an upper level anticyclone to the northeast which also moved westward. The sea level pressure field for 00Z 28 August is shown in Fig. 14. There is a relatively good correspondence between the NHC best track positions and those of Exp. A25 (e.g., 233 km difference at 72 h). The intensity of Exp. A25 was quite close to the best

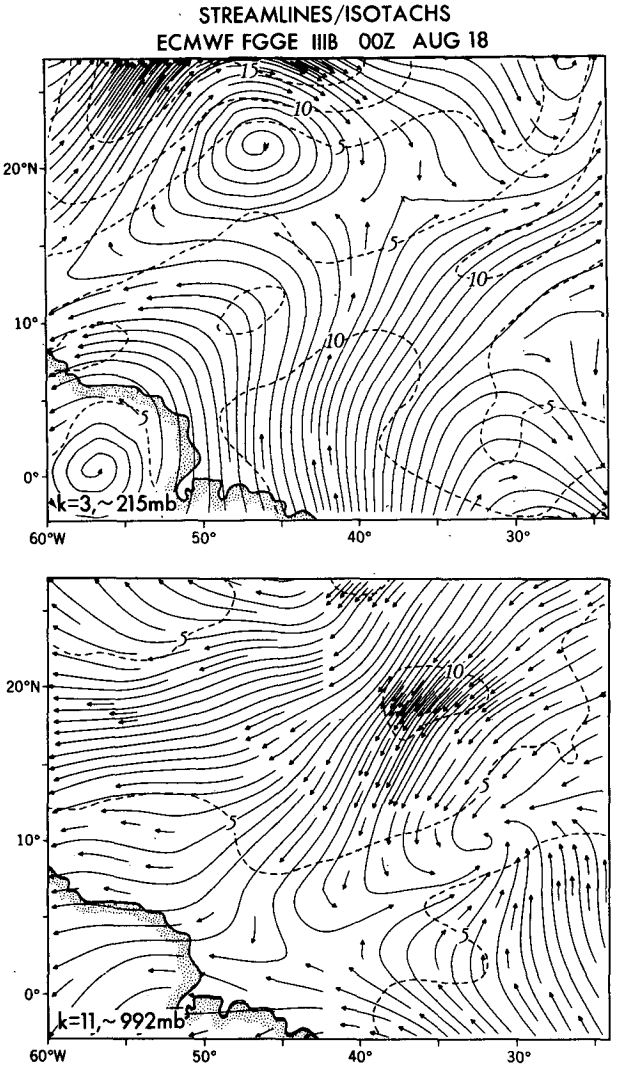

FIG. 7. Streamline and isotach analysis of the ECMWF FGGE IIIB dataset for 00Z 18 Aug 1979 for the regional domain of Exp. A18 (~215 mb, $k = 3$, upper; ~992 mb, $k = 11$, lower). Values of wind speed in m s^{-1}.

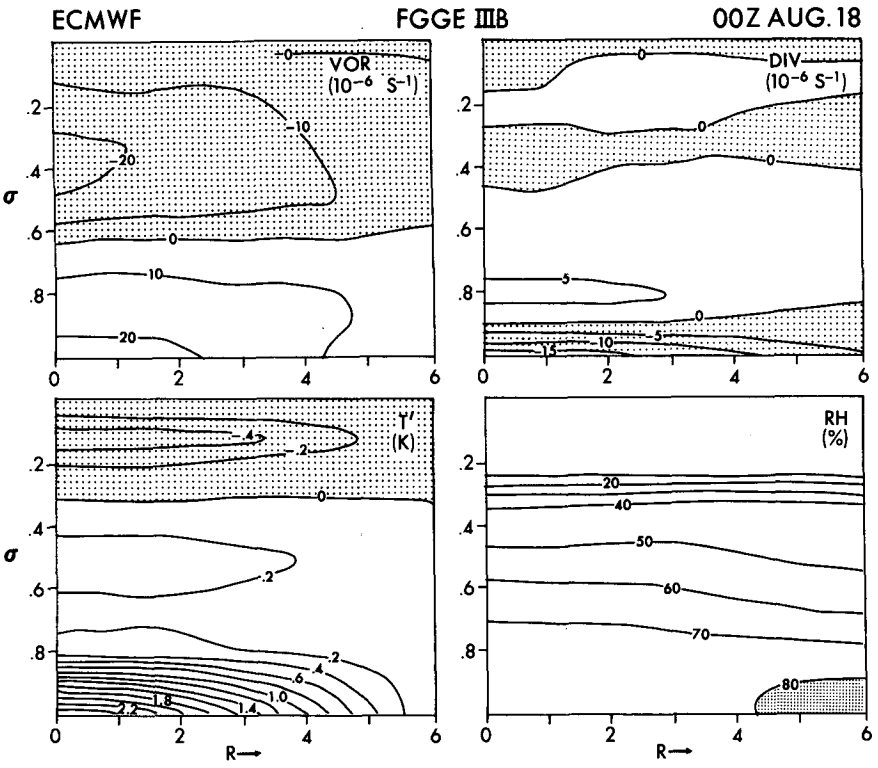

FIG. 8. Circular average cross sections of relative vorticity, divergence, temperature anomaly, and relative humidity for ECMWF FGGE IIIB for 00Z 18 Aug. The origin (10.0°N, 32.0°W) is taken from the disturbance center determined from the ECMWF data. The distance from the center is given in degrees latitude with each integer value being equivalent to approximately 111 km. The temperature anomaly is that related to the mean temperature at 6 degrees radius from the center.

track estimates for the first two days but the accuracy deteriorated after that (Fig. 10). Nevertheless Exp. A25 winds exceeded 30 m s^{-1}.

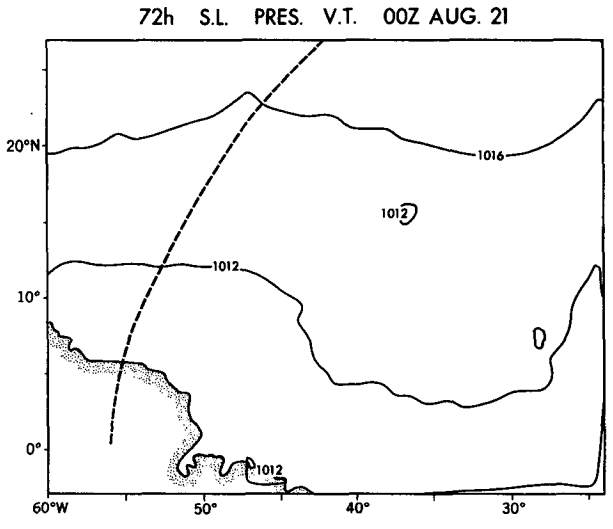

FIG. 9. The sea level pressure distribution of Exp. A18 for the verification time 00Z 21 Aug 1979. The dashed line is the trough position defined from the low level wind field of the ECMWF FGGE IIIB analysis.

d. A multistorm case in the Pacific in October

The last case study was that in the Western Pacific for the period 4 to 7 October. This period was selected because it was quite active and contained a multi-storm case. Tropical Storm Roger was located at 19°N, 137°E and Typhoon Tip was in its incipient stage on 00Z 4 October. Roger meandered for a day and moved to the north failing to reach hurricane strength. Tip, however, meandered for several days, slowly developing into a tropical storm. It later rapidly intensified into one of the most intense typhoons on record with a recorded pressure of 870 mb on 12 October. The initial sea level pressure field (Fig. 15) contains Tip in the southeast and Roger in the northwest of the specified domain. The cyclonic relative vorticity areas are associated with cyclonic wind fields of both these systems (Fig. 16). Aloft deep easterlies exist with the significant feature being an upper level cold low north of the incipient stages of Tip. At 00Z 4 October, the initial stage of Tip (Fig. 17) contains low level cyclonic vorticity extending to 300 mb with values of 20×10^{-6} s^{-1} extending to 500 mb and to 3.5° from the center. The divergence, temperature anomaly, and relative humidity cross sections indicate that Tip was already quite well organized with a deep, low level inflow, strong

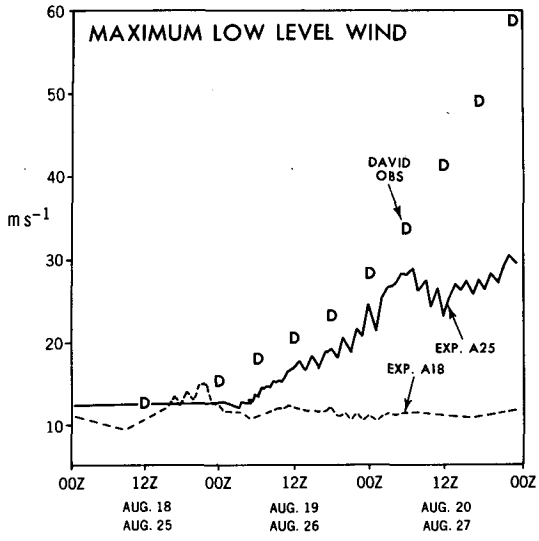

FIG. 10. The maximum low level wind at ~992 mb (k = 11) for Exps. A18 and A25 as a function of time. The NHC observations of David are given by the letter "D".

upper level outflow, a significant upper level warm anomaly, and high low level relative humidity.

In Exp. O04, the Tip depression erratically moved southwest for one day, then proceeded northwestward. As in the observed case, the depression was ill-defined for the first day and a half and it intensified quite slowly for the three day period. Notice that the initial analyzed position was ~350 km off from the JTWC best track position (Fig. 18). In Exp. O04, tropical storm Roger meandered near 20°N, 135°E before accelerating northward after one day and propagating through the domain boundary. Generally the track was well simulated although the strength of Roger was less than the JTWC estimates (Figs. 18 and 19). The model simulated movement of Tip was relatively accurate for two days although it did not simulate the tight cyclonic loop as was observed. The position error got progressively worse, increasing from 368 km at day two to 630 km at day three. Figure 19, however, illustrates that Exp. O04 accurately simulated Tip's slow intensification. Despite the slow growth, copious amounts of precipitation fell in Exp. O04 near Tip, near Roger, and in a cloud mass to the west of Tip and south of Roger. Notice that the outer circulation of Tip as de-

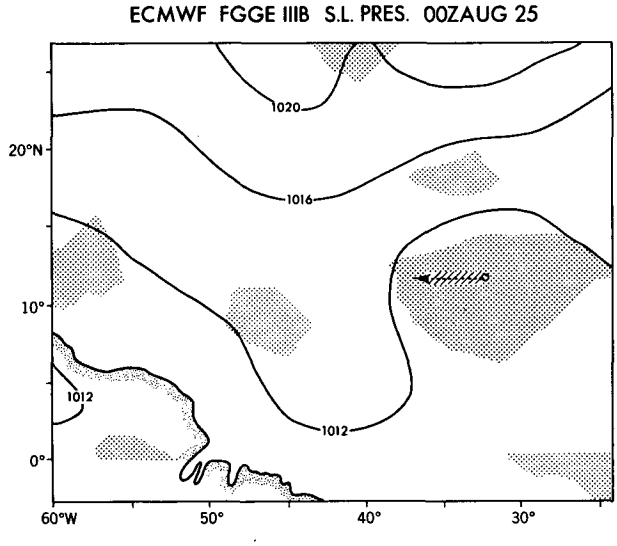

FIG. 11. The sea level pressure analysis of the ECMWF FGGE IIIB dataset for 00Z 25 Aug 1979 for the regional domain of Exp. A25. Shading indicates cyclonic vorticity greater than 10×10^{-6} s^{-1} at ~950 mb (k = 9). The arrow indicates the first reported best track fix of David by NHC at 12Z 25 Aug and its track is extrapolated back to the 00Z 25 Aug position indicated by the open circle.

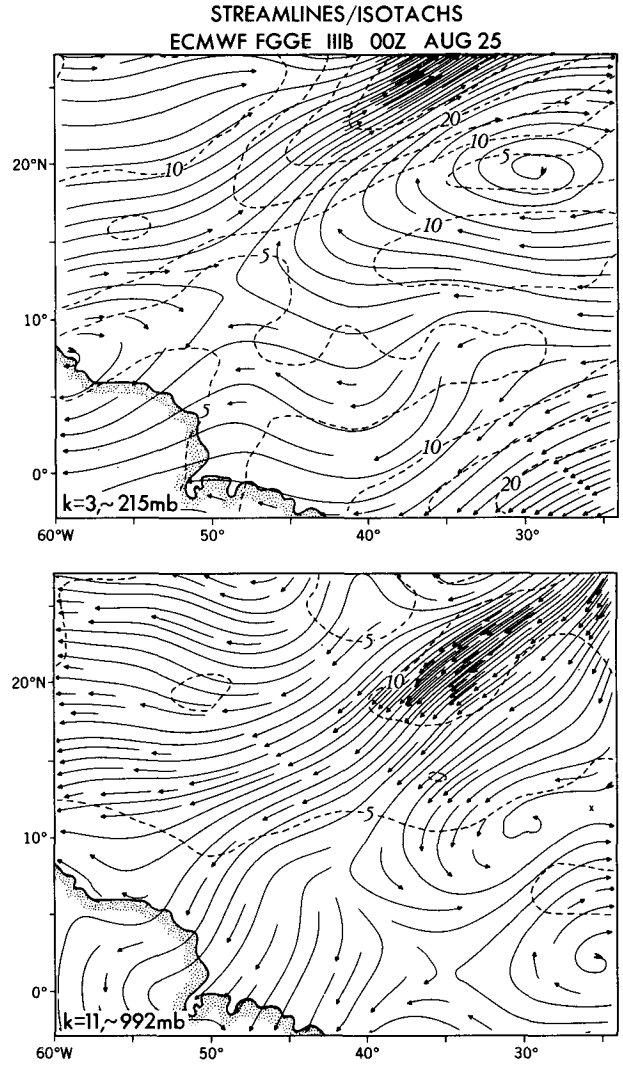

FIG. 12. Streamline and isotach analysis of the ECMWF FGGE IIIB dataset for 00Z 25 Aug 1979 for the regional domain of Exp. A25 (~215 mb, k = 3, upper; ~992 mb, k = 11, lower). Values of wind speed in m s^{-1}.

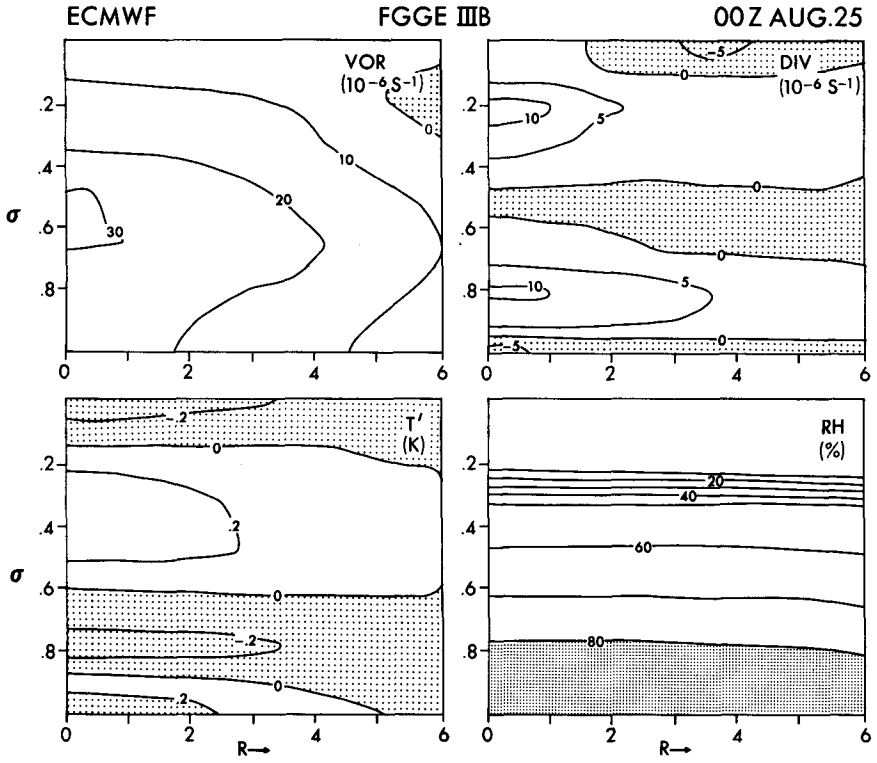

FIG. 13. Circular average cross sections of relative vorticity, divergence, temperature anomaly, and relative humidity for ECMWF FGGE IIIB for 00Z 25 Aug. The origin (8.8°N, 31.3°W) is taken from the disturbance center determined from the ECMWF data. The distance from the center is given in degrees latitude with each integer value being equivalent to approximately 111 km. The temperature anomaly is that relative to the mean temperature at 6 degrees radius from the center.

fined by the size of the outermost closed isobar showed no signs of constricting. In fact the circulation size increased as significant convection was common throughout this large area. In summary, Exp. O04 correctly simulated the slow intensification of Tip into a tropical storm with a large circulation. The simulation of the track was not as accurate as Exps. M05 and A25 but the observed track was quite complicated. The movement of Roger in Exp. O04 was also encouraging in that it simulated that storm's slow initial meandering and subsequent movement through the domain boundary.

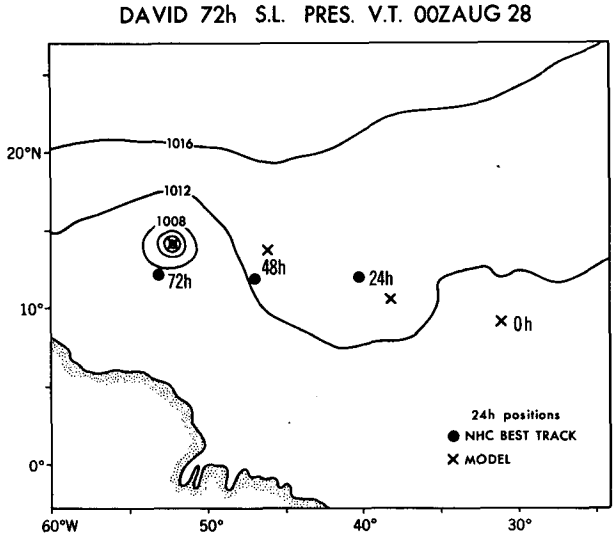

FIG. 14. The sea level pressure distribution of Exp. A25 for the verification time 00Z 28 Aug 1979. Daily storm positions of NHC observations and model are given by dots and X's respectively.

e. Summary

These experiments were successful in simulating the genesis of three pre-storm disturbances into tropical storms from an initial global scale FGGE analysis. In most cases the tracks were quite accurate despite the initial conditions being defined from large scale analyses which have apparent initial position errors. The intensification skill varied with each experiment although it seemed accurate to two days. It was also encouraging that it could simulate a slow, large development (Tip) as well as a rapid, small scale development (David). It was also demonstrated that a nondeveloping case could be correctly simulated. This case had a similar low level wind field to the developing case of David. Exp. O04 also demonstrated the ability

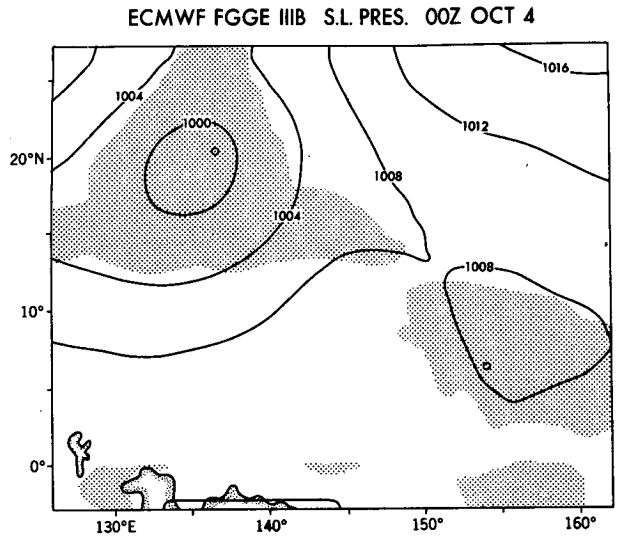

FIG. 15. The sea level pressure analysis of the ECMWF FGGE IIIB dataset for 00Z 4 Oct 1979 for the regional domain of Exp. O04. Shading indicates cyclonic vorticity greater than 10×10^{-6} s^{-1} at ~950 mb (k = 9). The reported best track positions of Roger and Tip by JTWC at 00Z 4 Oct are indicated by open circles.

of the model to handle a multiple storm case with a tropical storm moving through the domain boundary.

These results indicate that an incipient storm's evolution is influenced by large scale deterministic environmental conditions, at least one day prior to the observation of storm force winds. As suggested by Ooyama (1982), this may be questionable at an earlier stage of formation when the evolution of a mesoscale system of organized convection can be probabilistic in nature. From a practical view, however, the precise point in time to separate these two stages may be difficult to determine.

4. Features of the simulated tropical disturbances

In the preceding section, a description of the simulation experiments of individual storms was given which emphasized the storm tracks, final state pressure field and the gross disturbance intensification rate as defined by the maximum low level wind. Comparison was also made to the best track observation. We will now look at more details of these simulations such as precipitation patterns and storm structure both during intensification and at the final state. Also discussed will be the kinetic energy, moisture, heat, and vorticity budgets. Only the most pronounced features will be highlighted.

a. Precipitation patterns and storm structure

One interesting finding was the remarkable correlation between the model simulated precipitation fields and observed infrared cloud images. In general the correlation is quite good through 36 h. Two cases will be presented here although all cases indicated agreement. The model precipitation at 24 h in Exp. A18 is compared to the satellite photo after 00Z 19 August in Fig. 20. This is the period of peak activity for the cloud cluster that was simulated with precipitation rates exceeding 30 mm h^{-1} in the model. The model accurately simulates the disturbed region between 5°–10°N and 40°–30°W and its northward extension at 30°W to north of 10°N. Also evident is the smaller cluster to the west at 45°–50°W. Experiment A18 even has some hint of precipitation at the northwest corner of the domain.

Another example of the model precipitation forecast skill is shown in Fig. 21 from Exp. O04. The satellite

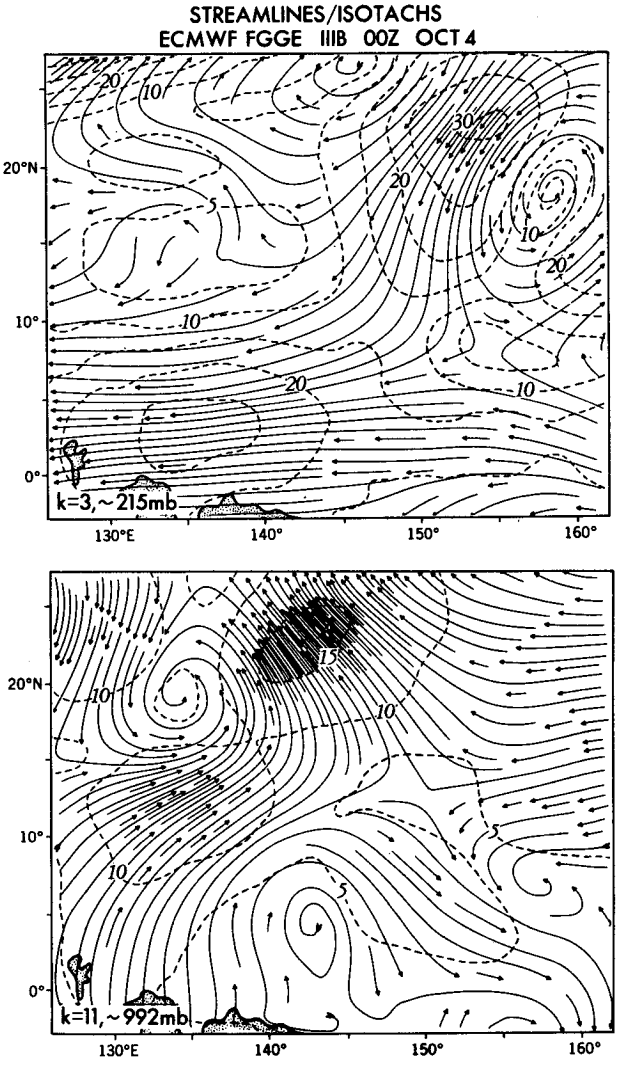

FIG. 16. Streamline and isotach analysis of the ECMWF FGGE IIIB dataset for 00Z 4 Oct 1979 for the regional domain of Exp. O04 (~215 mb, k = 3, upper; ~992 mb, k = 11, lower). Values of wind speed in m s^{-1}.

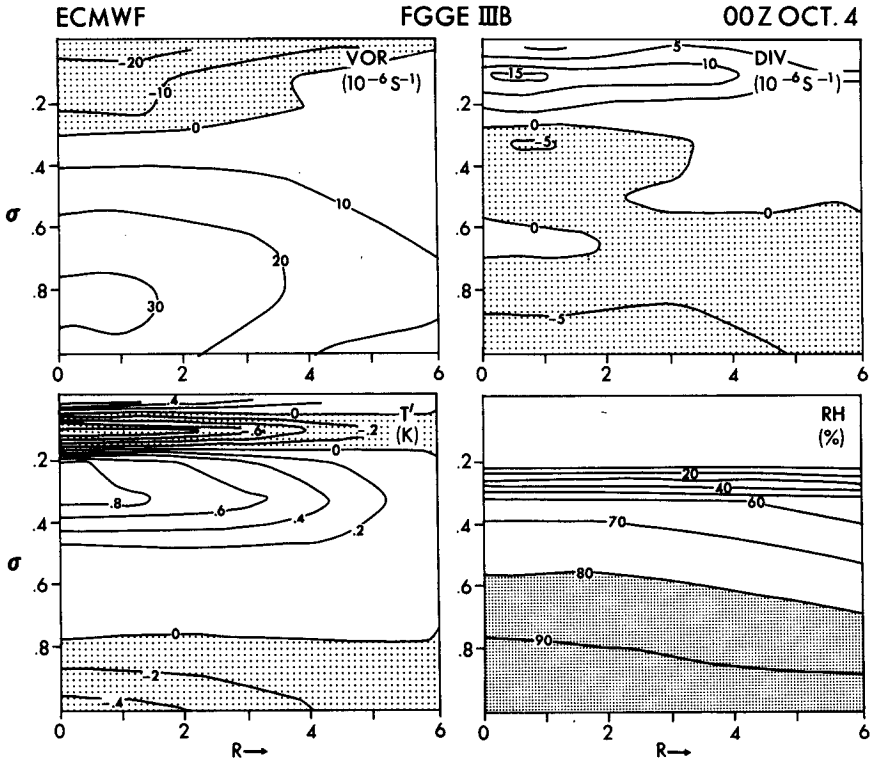

FIG. 17. Circular average cross sections of relative vorticity, divergence, temperature anomaly, and relative humidity for ECMWF FGGE IIIB for 00Z 4 Oct. The origin (9.2°N, 155.7°E) is taken from the disturbance center of Tip determined from the ECMWF data. The distance from the center is given in degrees latitude with each integer value being equivalent to approximately 111 km. The temperature anomaly is that relative to the mean temperature at 6 degrees radius from the center.

photo is taken for the period 04Z 5 October. At this time Tip was located at (5.6°N, 155.0°E) and Roger at (20.2°N, 134.9°E). A third disturbed region lies between these two disturbances. The model simulated rather accurately not only the regions of precipitation but also details such as the line orientation of Roger's

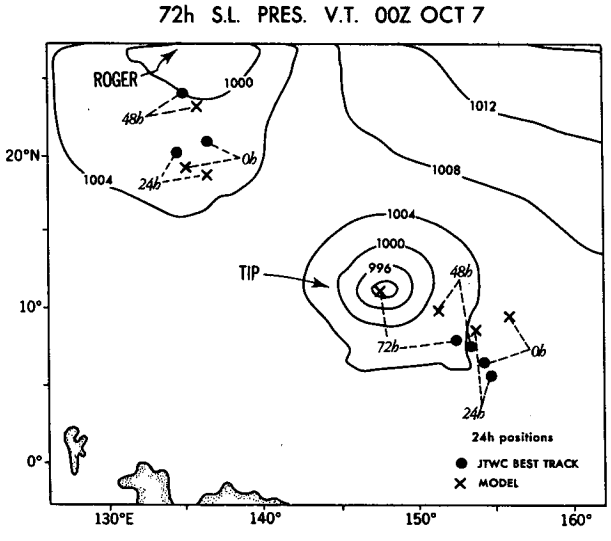

FIG. 18. The sea level pressure distribution of Exp. O04 for the verification time 00Z 7 Oct 1979. Daily storm positions of JTWC observations and model are given by dots and ×'s respectively.

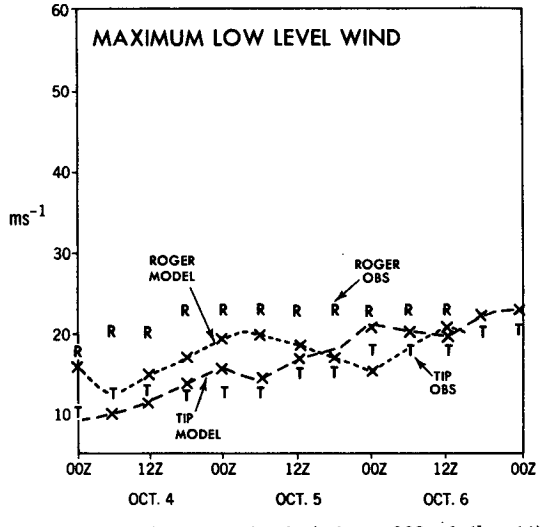

FIG. 19. The maximum low level wind at ~992 mb (k = 11) for Exp. O04 as a function of time for Roger (dotted) and Tip (dashed). The JTWC observations of Roger and Tip are given by the letters "R" and "T" respectively.

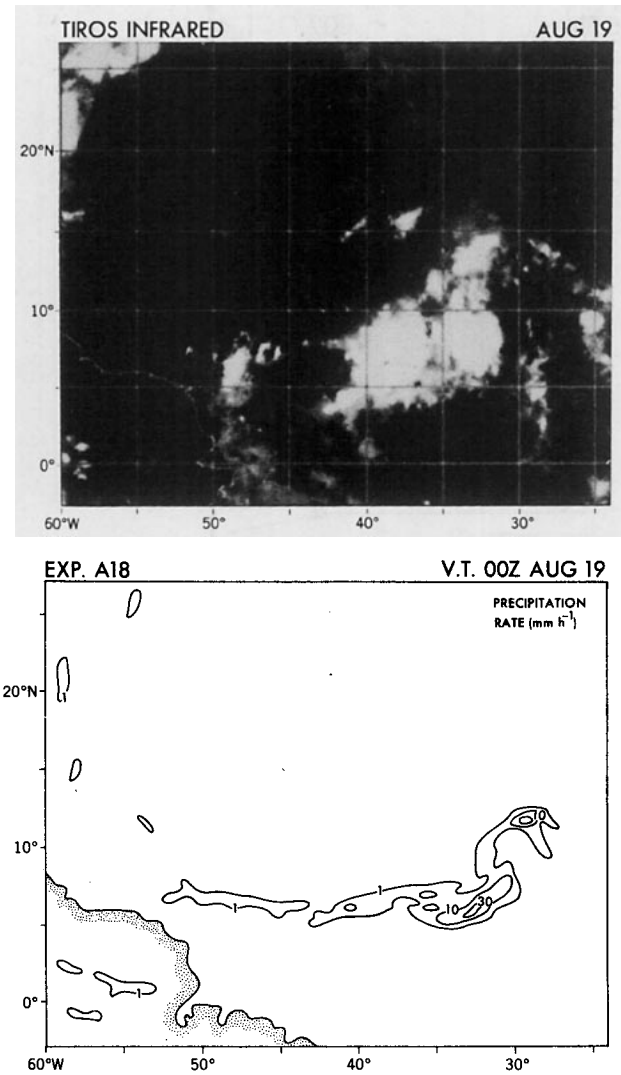

FIG. 20. Infrared satellite photo (top) and Exp. A18 precipitation rate (bottom) valid at 00Z 19 Aug 1979, 24 h into the Exp. A18 simulation.

precipitation and holes in Tip's pattern, and the sharp cutoff north of the third disturbance region. It is unclear from satellite photos but the model simulation implies that the cloud region of the third area may be primarily a cirrus shield. The upper level winds are blowing outward, anticyclonically from Roger southwestward over this precipitation area simulated by the model. Another feature is the relatively large extent of model precipitation and observed huge cloud mass associated with the Tip development. This can be contrasted with the more isolated observed cloud mass and model precipitation pattern associated with David (not shown). Also note the strong correlation between the model simulated rain free areas and the corresponding cloud free areas in the satellite photo. Comparisons of model precipitation against satellite clouds were made both for other times and the two other case studies and in forecast mode experiments as well, and they indicate the above results can be generalized. This leads to the speculation that at least in some cases, mesoβ (20–200 km) scale convective activity can be forecasted reasonably well from an initial large scale environment resolvable in a global analysis.

The model's ability to form band type patterns is another feature of these experiments. One can investigate the banding at a later stage in the simulation although its correlation with satellite photos may not be as accurate. The banding is observed in low level vorticity, precipitation, temperature, wind speed and other fields. The relationship is similar to that found by Tuleya and Kurihara (1984) except that now the bands tend to be smaller probably due to the finer resolution. One example of banding is in the precipitation

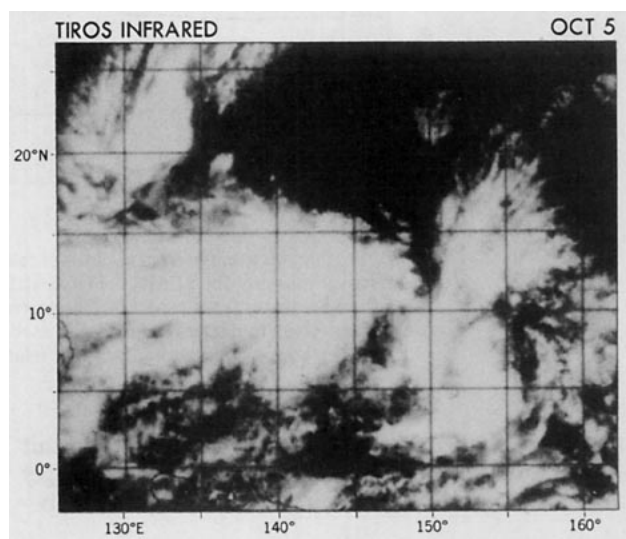

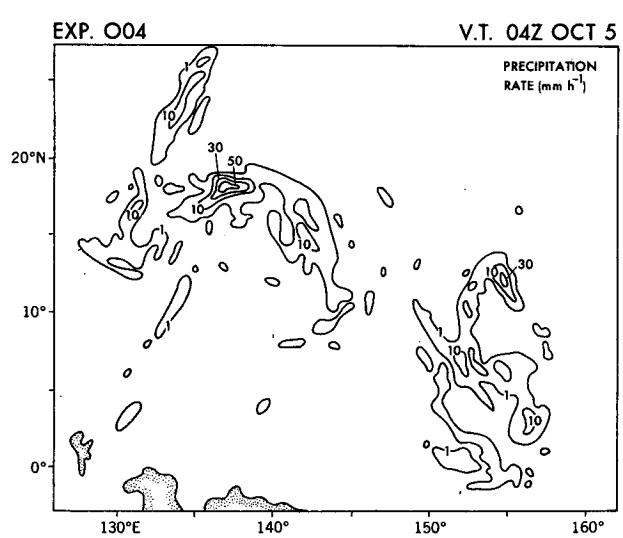

FIG. 21. Infrared satellite photo (top) and Exp. O04 precipitation rate (bottom) valid at 04Z 5 Oct 1979, 28 h into the Exp. O04 simulation.

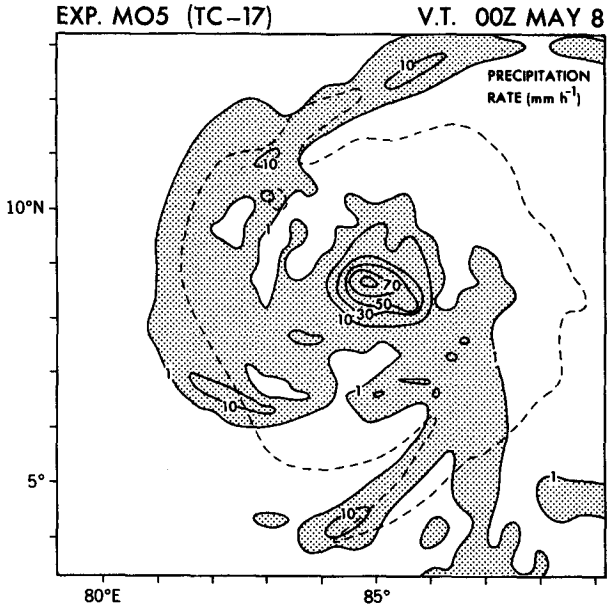

FIG. 22. Precipitation rate of Exp. M05 for the storm, TC-17, valid at 00Z 8 May 1979, 72 h into the simulation. Values greater than 1 mm h^{-1} are shaded. Also shown is the 14 m s^{-1} contour (dotted line) of the wind speed at ~992 mb (k = 11).

at 72 h for Exp. M05 verifying at 00Z 8 May (Fig. 22). One band extends in front of the westward moving cyclone to the southwest, then to northwest and northeast 400 km from the storm core. A second band extends southeast from the storm then to the south (anticyclonically). The main core precipitation rate exceeds 100 mm h^{-1}. There is a tendency for a wind speed maximum at the leading edge of the precipitation band (shaded area of Fig. 22). These bands appear similar to the stationary complex described by Willoughby et al. (1984) in that the bands show little propagation relative to the moving storm. The resolution is not fine enough to resolve small scale rainbands which may be embedded in these relatively large scale (50–100 km) features. Furthermore, cloud scale processes not considered in the present model could certainly influence the behavior of these bands. There is a similar tendency for bands of various strengths in the cyclones of Exps. A25 and O04.

The final stage structure of the simulated developing storms varied from case to case. This is evident from the variety of sea level pressure patterns given in section 3. To emphasize this difference we will concentrate on the structural differences between the simulation of David, Exp. A25, and that of Tip, Exp. O04 (Fig. 23). One can see a dramatic size difference in these two storms. In the case of Tip, winds greater than 16 m s^{-1} (shaded regions of Fig. 23, bottom) extend beyond 350 km from the center while less than 200 km in the David simulation. From the initial wind patterns of Figs. 12, 13, 16 and 17, it is not evident that Tip's circulation was initially larger than David's although differences in detail certainly exist in the wind field. Tip was more moist in terms of both relative and absolute humidities. Convection was more widespread in Exp. O04 in the developing stages (Fig. 21) than in Exp. A25 and vertical wind shear was more prevalent. These factors could contribute to storm size differences but in what manner it is not obvious.

Another difference between these two developing storms are the relative positions of the low level max-

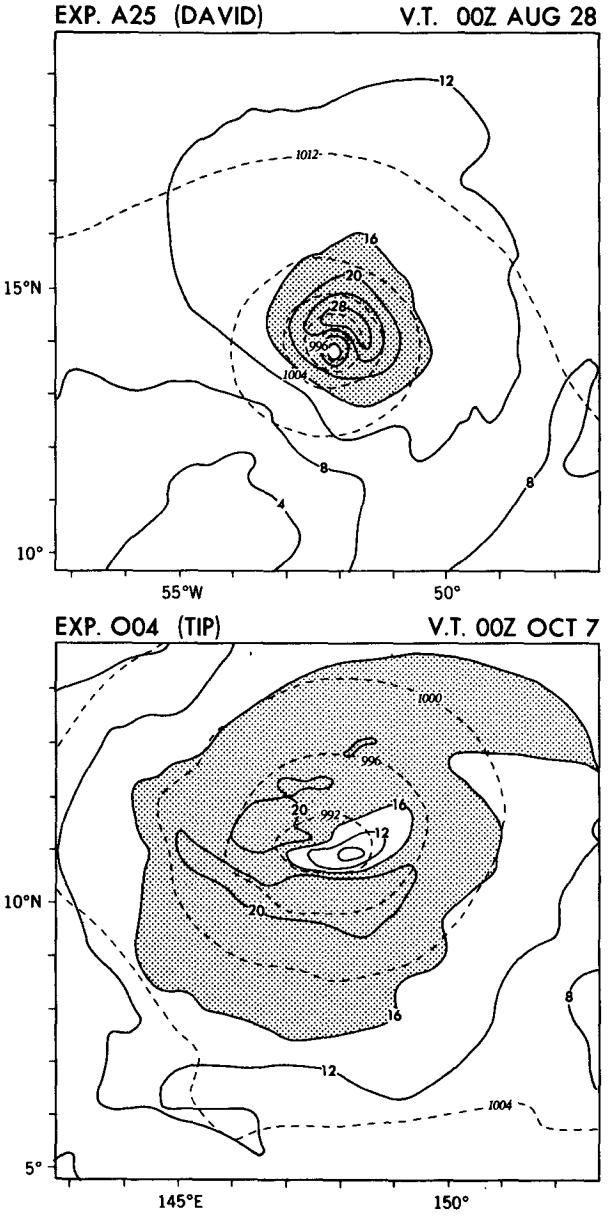

FIG. 23. Low level wind speed at ~992 mb (k = 11) at 72 h for the storm, David, valid at 00Z 28 Aug 1979 (top) in Exp. A25 and for the storm, Tip, valid at 00Z 7 Oct 1979 (bottom) in Exp. O04. Values greater than 16 m s^{-1} are shaded with sea level pressure indicated by dashed lines.

imum winds. In Exp. A25, the maximum winds are more classically positioned toward the right and right rear (Shea and Gray 1973; Tuleya et al. 1984). Experiment O04 displays two wind maxima, one close to the center to the south, another extending from just northwest of the center to the northeast. This second band has distinct precipitation and vorticity bands associated with it. Although not shown, the vertical structure of each case is distinct. In Exp. A25, the storm warm core at ~335 mb is immediately above the surface pressure center and the cyclonic circulation extends up through 300 mb. The warm core at ~335 mb in Exp. O04 is located just to the west of the pressure center and is consistent with the easterly flow found above the center. Despite Tip's large size and precipitation abundance, the cyclonic circulation does not yet extend to the upper troposphere.

One can conclude that a variety of storm structures exists in the model simulations as in reality. Storms can vary in size, wind and precipitation distributions, and vertical structure. In these simulations this variety originates from the large scale environmental flow and the resolvable structure of the original incipient disturbance.

b. *Development criteria*

We have seen in the previous section that development occurs in some cases (Exps. M05, A25, and O04) and not in another (Exp. A18). In addition the developing storms did not all develop at the same rates. From the previous discussions one could attribute these differences to moisture availability and disturbance structure. Some features of the early characteristics of the four simulated tropical disturbances are summarized in Table 2. As in McBride and Zehr (1981), all the cases contained low level cyclonic vorticity and upper level warm anomalies. We will now look at various development criteria in more detail.

Vertical wind shear of the environment has been known to influence storm evolution by observational studies (Gray 1968) and numerical simulation (Tuleya and Kurihara 1981). Figure 24 gives the area averaged (15° × 15°) vertical profiles for the zonal, u, and meridional, v, wind at 12 h of Exps. M05, A18, A25 and O04 as well as the corresponding phase speed of the disturbances as measured by the movements of the pressure centers for the corresponding experiments. Notice again the variety of mean flow conditions from case to case. Monsoon westerlies prevail at low levels in Exps. M05 and O04 while deep easterlies are present in Exp. A25. A week earlier than the time of Exp. A25 in the Atlantic, i.e., in Exp. A18, easterlies were not as prevalent with little sign of easterly mean flow. The meridional circulation indicates a Hadley type circulation in Exp. O04 and to a lesser extent in Exps. M05, A18, and A25. In this study the zonal component of propagation is westward for all the disturbances. All developing cases display easterly vertical shear [i.e., $U(\sigma = 0.2)-U(\sigma = 0.8) < 0$] from the surface boundary layer to the tropopause. The nondeveloping case of Exp. A18 contains evidence of protrusion of westerlies

TABLE 2. Initial characteristics of the simulated tropical disturbances.

Case	Exp. M05 (5 May)	Exp. A18 (18 Aug)	Exp. A25 (25 Aug)	Exp. O04 (4 Oct)
Development	Yes	No	Yes	Yes
Low level vorticity	Deep cyclonic	Shallow cyclonic	Deep cyclonic	Deep cyclonic
Upper level vorticity	Anticyclonic	Anticyclonic	Cyclonic	Anticyclonic
Associated upper level disturbance	Anticyclone northeast of surface disturbance	Anticyclone east of surface disturbance	None	Cold upper level low to north
Relative humidity	>90% near center in shallow layer	<80% near center	>80% at low levels	>80% in deep layer above sfc.
Upper level warm anomaly (~335 mb)	East of sfc. disturbance	East of sfc. disturbance	Over disturbance and north	Over disturbance
Environmental (15 × 15 deg) vertical shear	Moderate easterly shear	Southwesterly shear	Weak easterly shear	Strong easterly shear
Environmental (15 × 15 deg) vertical motion at 12 h	Downward +3 mb h^{-1} at midlevel	Upward −3 mb h^{-1} at 700 mb	Upward −1 mb h^{-1} at 800 mb	Upward < −7 mb h^{-1} at midlevel
Environmental (15 × 15 deg) heating distribution at 12 h	Horizontally confined penetration	Penetrative heating	Confined to low levels	Large, deep heating

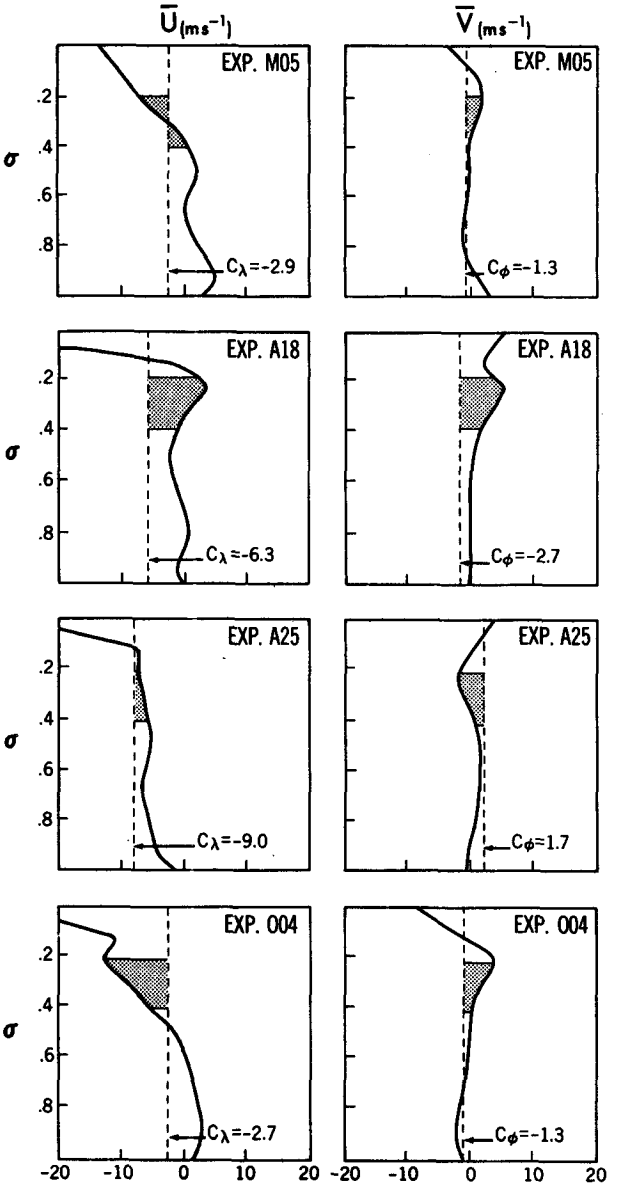

FIG. 24. Domain average zonal, u, and meridional, v, components of the wind at 12 h for Exps. M05, A18, A25 and O04 for a 15° × 15° area centered on the low level incipient disturbance. Positive (negative) values of u indicate westerlies (easterlies) while positive (negative) values of v indicate southerlies (northerlies). Also shown are the zonal and meridional phase speeds of the disturbances (dashed lines). Shading indicates departure of upper level winds from the phase velocity of the disturbances.

at ~300 mb. The rapidly developing systems (Exps. M05 and A25) also display a strong vertical coupling of the phase speed of the disturbance and the upper level winds whereby the disturbance propagates with the same velocity as the upper level winds. This coupling is indicated by the relatively small departure of the upper level winds from the phase speed as shown by the shading in Fig. 24. It may be speculated that the slow amplification of Tip may be due in part to the strong easterly shear that exists in this case. This analysis confirms the previous work of Tuleya and Kurihara (1981) that storm genesis can be hindered or retarded when the phase speed is not coupled with upper level winds. A recent study by Yamazaki and Murakami (Meteorological Research Institute, Japan Meteorological Agency, personal communication) indicates that active periods of the FGGE year in the tropical Pacific were associated with anomalous easterlies aloft and westerlies at the surface. The anomalies were associated with a period of ~30 days and zonal wave number 4–6.

c. *Heat, kinetic energy, moisture, and vorticity budgets*

One can also investigate the development rates by looking at the model heating tendency and subsequent warm core evolution as well as the kinetic energy, moisture, and vorticity budgets of the various cases. Again a wide variety of evolutions make generalization difficult. In the evolution of the warm core, a warm area often exists prior to genesis, but seldom directly over the low level disturbance center. The intensification of the upper-level warm area into a warm core and its coupling with the low level disturbance was gradual in the case of David with the process taking a day or two while in TC-17 a warm core became established in less than a day. In the heating tendency of the model simulation it was found by Kurihara and Tuleya (1981) that a delicate balance exists between cooling due to upward motion and convective heating. Often in the present cases a horizontal offset exists whereby warm core formation takes place not at the position of maximum convective heating and upward motion but at the center of low level circulation. In Exp. A18, however, the low level circulation was coincident with the center of the upward motion area. In Exp. M05, the development ensued in an environment where the mean vertical motion, averaged for a 15° × 15° area centered on the disturbance, was downward. In this case, only in a small area did upward motion exist through low level convergence. Therefore environmental vertical motion may not always be a good indicator of genesis.

Kinetic energy and moisture budgets were computed for each simulation following the method of Tuleya et al. (1984). The kinetic energy equation for a 5° × 5° domain following a storm may be written as:

$$\overline{\frac{\partial}{\partial t}\int p_*(u^2+v^2)/2d\sigma/g} = \overline{-\int \nabla\cdot[(\mathbf{V}-\mathbf{C})p_*(u^2+v^2)/2]d\sigma/g} - \overline{\int p_*\mathbf{V}\cdot\nabla_p\phi d\sigma/g} + \overline{\int p_*\mathbf{V}\cdot\mathbf{F}_v d\sigma/g} \quad (4.1)$$

The overbar denotes the storm area average, p_*, the surface pressure, u and v the zonal and meridional components of the wind, **V**, and **C** is the phase velocity. In addition $\nabla_p\phi$ is the pressure gradient and $\mathbf{F}_v$ is the diffusive tendency of momentum due to subgrid scale processes. The term on the left of (4.1) is the kinetic energy tendency and the terms on the right are conventionally referred to as the flux convergence, generation, and dissipation of kinetic energy respectively. Budget terms are given for Exps. A18 (nondeveloping), A25 (David) and O04 (Tip) in Fig. 25. The dissipation terms, significant negative components in the kinetic energy budget, are not plotted because they are similar in form to the kinetic energy terms (Fig. 25, bottom). Notice that the Tip kinetic energy is consistently greater than that of David. This is consistent with the overall size difference between the two storms. The kinetic energy and maximum surface wind speed tendencies are in qualitative agreement (Figs. 10, 19 and 25). In the top part of Fig. 25, one sees that the generation term is relatively more important for Exp. O04. On the other hand the amount of flux convergence of kinetic energy into the storm area for Exp. A25 is significant compared to the generation at the time of intensification (~36 h). For Exp. O04, the influx of kinetic energy at lower levels was found to be offset by upper level divergence of kinetic energy. In Exp. A18, after some small initial increase in kinetic energy to 24 h, there was a decrease of kinetic energy to values below that of Exp. A25. The generation term of Exp. A18 showed a decrease from 12 to 48 h while the flux convergence of kinetic energy was found to be negative before 24 h and negligible afterward. In Exp. M05 (not shown here), both kinetic energy and its generation showed an exponential increase while the flux convergence term played a minor role.

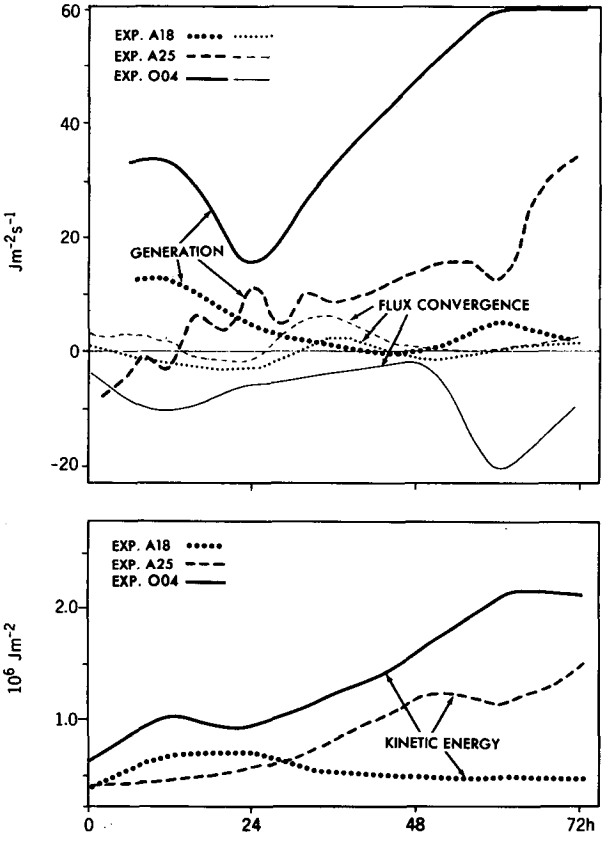

FIG. 25. Time history of the generation (heavy line) and flux convergence (thin) components of the kinetic energy budget (top) for Exps. A18 (dotted line), A25 (broken) and O04 (solid) for a 5° × 5° area following the storm. The dissipation and diffusive flux convergence terms are not plotted. The kinetic energy is also shown (bottom).

A moisture budget equation may be written for the same moving 5° × 5° area following the storm as

$$\frac{\partial}{\partial t}\int p_* r\,d\sigma/g = -\int \nabla\cdot(\mathbf{V}-\mathbf{C})p_* r\,d\sigma/g + \overline{\text{EVAP}} - \overline{\text{PREC}} + \overline{\text{HDIF}} \quad (4.2)$$

where r is the mixing ratio, EVAP is the evaporation, PREC is the precipitation, HDIF is the diffusive convergence of precipitable water, and the other symbols have been defined previously. The integral on the left defines the precipitable water, PRECW, while the integral on the right defines the convergence of moisture into the domain, CONVERG. Water vapor budgets were performed for each simulation. Table 3 summarizes the results into early stage (12–36 h) and later stage (48–72 h). In all cases there is a rough balance between the two moisture sources, horizontal flux convergence and surface evaporation of moisture and the precipitation sink. Notice that for the first stage Exp. A18 displays more precipitation and evaporation than Exp. A25. Also notice that the evaporation rate did not increase for the nondeveloping case but did for the other developing cases. Also the precipitable water content of A18 was significantly less than the developing cases and that it reduced even more in the second period. It appears that the nondeveloping disturbance managed to have copious amounts of precipitation initially due to low level convergence but quickly dried out because the environmental flow was not conducive to import more moisture.

Vorticity tendencies were computed for various development times of the simulation experiments. Generally the results are similar to Kurihara and Tuleya (1981) in that the stretching term contributes to low level vorticity increase and horizontal advection contributes to the concentration of low level vorticity to the disturbance center in Exps. A25 and M05. In Exp. A18 the net positive tendency and stretching term were not aligned with the surface center.

d. Summary

In summary convective heating and upward motion alone are not enough to explain genesis. The warm core results from a combination of horizontal and ver-

TABLE 3. Moisture budget for two stages of the experiments for a 5 × 5 deg. domain centered on the moving disturbance. Values, an average of three instantaneous times at 12 h intervals, are expressed in equivalent water depth. The tendency terms may be converted to cm h^{-1} by multiplying by 0.036.

	12–36 h				48–72 h			
Exp.	Precipitation	Convergence (10^{-7} m s^{-1})	Evaporation	Precipitable water (10^{-2} m)	Precipitation	Convergence (10^{-7} m s^{-1})	Evaporation	Precipitable water (10^{-2} m)
M05	9.5	7.4	0.4	5.7	13.4	10.3	1.0	5.7
A18	5.3	4.4	0.4	5.1	1.2	0.5	0.3	4.6
A25	3.0	2.6	0.3	5.4	7.8	5.1	0.6	5.5
O04	9.7	7.7	0.5	6.1	13.9	10.4	1.2	5.8

tical motions and convective heating. Moisture supply from both the horizontal import and surface evaporation is found important from investigation of the moisture budget. The kinetic energy budget indicates that the generation term dominates the increase in kinetic energy in most cases but in Exp. A25 an influx of energy was important at the time of early intensification. Important terms in the low-level vorticity tendency are the stretching and relative horizontal advection although the vorticity change is quite nonlinear and difficult to interpret. Additional analyses and experiments may be needed to isolate the precise role of potential individual genesis mechanisms including convective instability, air–sea interaction, low level wind surges, upper level outflow channels, tropical upper tropospheric troughs, and other nonlinear interactions.

5. Summary and conclusions

This study demonstrates that tropical storm genesis can be simulated using a fine resolution (¼° × ¼°) regional model and an adequate initial condition based on a large scale analysis. This investigation also demonstrates the importance of the surrounding environment in controlling the intensification of an incipient disturbance into a tropical storm. Several cases were investigated ranging from an easterly wave development in the Atlantic to monsoonal trough developments in the Pacific and Indian Ocean. Also simulated was a nondevelopment in the Atlantic in which the low-level wind field was initially quite similar to the developing case. It was shown in these cases that the simulated intensification rate may not be accurate especially after two days. The simulated track positions compared well to both observation best track fix position and operational forecasts made a day or two later, although there was a wide variation from case to case.

Another encouraging result is the model's ability to simulate detailed storm structure similar to those observed. The simulated storm size ranged from a small, compact storm in David to a huge circulation in Tip. Banding of wind, moisture, and precipitation fields was a common occurrence in these simulation experiments. Cloud patterns observed compared well to model precipitation patterns through the second day of the simulation. This gives further evidence that the environmental scale analyzed by the FGGE data controls the evolution of storm development to some degree.

From these case studies, it is somewhat difficult to isolate the relative roles of various processes proposed in tropical cyclone genesis. However, this study did confirm what prior numerical and observational evidence have found empirically: Genesis originates from a region of existing cyclonic low-level vorticity and high moisture. Upper level ventilation is minimized in developing cases by a coupling of the upper level wind with the movement of the low level disturbance. For westward moving disturbances this leads to easterly vertical wind shear in the environmental wind being favorable for genesis. This study also emphasized that prevailing environmental vertical motion may not always be a good predictor of genesis.

The problem of predictability of genesis demands further research. This topic is addressed briefly in the Appendix that follows. Initialization of the analysis fields also may give an improvement in forecasting. More work needs to be done on the effects of lateral boundary conditions as well as the temporal sensitivity of the results. Other topics left for further research include the sensitivity of the results to the surface boundary conditions such as SST and topographical resolution.

Acknowledgments. The author would like to thank J. Mahlman, director, and Y. Kurihara, project head, for their continuous support for this investigation at GFDL. L. Lahiff, M. Lawrence of NHC/NWS and Y. Kurihara and K. Miyakoda of GFDL read an earlier version of this manuscript and gave invaluable suggestions for its improvement. They are grateful to J. Ploshay, W. Stern, and K. Miyakoda for providing advice on implementing FGGE data, and for providing the R30L18 spectral model. Best track and operational forecast data were expediently provided by A. Pike and M. Fiorino. D. Golder, R. White, G. Vandenberghe, N. Nakamura, and M. DiPaola deserve thanks for aid in the FGGE data processing. Special thanks and credit is also given to P. Tunison, K. Raphael, J. Varanyak, M. Zadworny and J. Conner for preparing the figures.

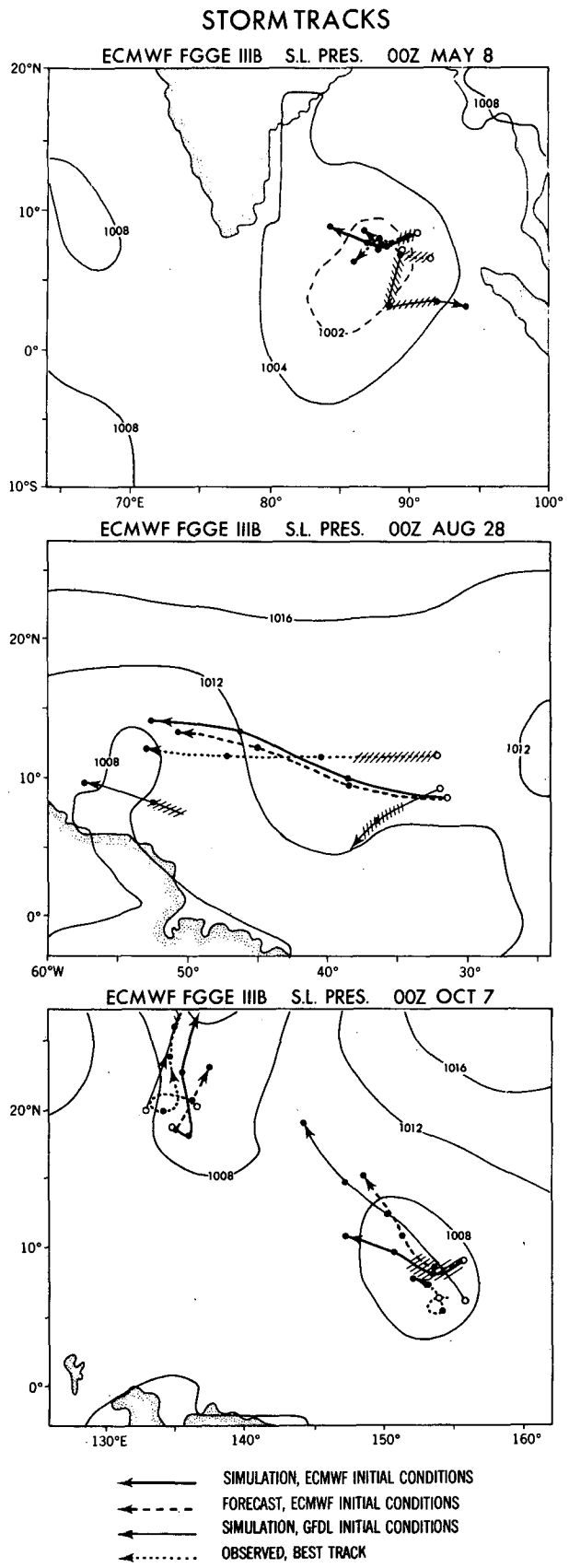

FIG. 26. Storm tracks for Exps. M05 (solid), M05F (dashed), M05G (thin solid), and best track of TC-17 (dotted), top; storm tracks for Exps. A25 (solid), A25F (dashed), A25G (thin solid), and best track of David (dotted), middle; storm tracks for Exps. O04 (solid), O04F (dashed), O04G (thin solid), and best track of Roger and Tip (dotted), bottom. Hatching indicates that tracks are uncertain. Daily positions are indicated by dots with the initial storm position for each experiment or estimated observed fix given by an open circle.

APPENDIX

Sensitivity Studies

In the text we have emphasized the set of experiments in which ECMWF FGGE IIIB analysis was utilized both as initial conditions and for the time dependent lateral boundary conditions. Besides the quality of the regional model itself, the predictability of genesis using this experimental design is a function of the quality of initial conditions and the quality of the large scale forecast at the regional domain boundaries. In this section, the sensitivity of the results to lateral boundary conditions and initial conditions are briefly discussed.

1. Impact of lateral boundary conditions on predictability

Experiments M05F, A18F, A25F and O04F were run with exactly the same initial conditions as Exps. M05, A18, A25, and O04; however, the time dependent lateral boundary conditions were obtained from the GFDL R30L18 spectral forecast Exps. M05S, A18S, A25S and O04S. As in the regional model experiments, the ECMWF FGGE IIIB dataset was used as initial conditions for the spectral model. In general this low resolution model can not forecast the intensification nor storm tracks for the Indian (TC-17) and Pacific Ocean (Tip and Roger) case studies. On the other hand, the forecasts of David's track and the nondeveloping wave compare favorably to both observations and the regional model simulation Exps. A25 and A18.

The tracks of the forecast mode experiments can be compared to the simulations for the developing cases in Fig. 26 (dashed vs thick lines). Any differences are attributable to the relative accuracy of the spectral model forecasts at the regional domain boundaries. In general the differences in track are relatively small to 48 h and then they diverge. The 72 h position errors of the forecasts for TC-17, David, and Tip in Exps. M05F, A25F, and O04F were 284, 312 and 911 km respectively. These errors were greater than those of the corresponding simulation mode in the cases of David and Tip, but less than those in TC-17.

A direct comparison with the operational forecasts is not possible since operational centers did not normally forecast position at such an early stage. However, one can compare these figures to the earliest official forecast verifying at day three. The JTWC had a 375 km error for a 34 h forecast of TC-17 and a 256 km

error for a 48 h forecast of Tip. The NHC made a 32 h forecast of David with an error of 296 km. Considering the early stage in which the forecasts were made, the track forecasts with the regional model were encouraging except for the obvious failure to predict the observed looping of Tip.

Besides track, the sensitivity of storm intensity to lateral boundary conditions was investigated. Using the forecast mode and ECMWF initial conditions, genesis was forecast in the three developing cases and the nondeveloping case was forecast not to develop. However, the Exp. A25F forecast of David was weak and too slow in developing compared to both observation and the Exp. A25 simulation. Tip, on the other hand, was forecast to be too intense in Exp. O04F. The forecast of TC-17, Exp. M05F, was actually more accurate than the simulation mode in both track and intensity. Some analysis of these results reveal that the intensity differences may be partially attributable to differences in domain scale vertical motion. This requires further investigations and more forecast experiments.

2. Impact of initial conditions on predictability

The initial conditions can have a dramatic impact on the track results. The simulations with GFDL FGGE IIIB consistently fail to capture the track direction with incipient TC-17 propagating to the south, then east (Exp. M05G); David disintegrating and reforming (Exp.A25G); and Tip and Roger accelerating too rapidly to the northwest and north respectively (Exp. O04G; Fig. 26, thin solid lines). The intensity of the tropical disturbances was also found to be quite sensitive to the initial conditions. For the GFDL FGGE IIIB initial conditions, only in Exp. O04G did the initial disturbance develop into a tropical storm and in that case the intensity of Tip was too large.

As mentioned previously, the GFDL analysis is being redone for the special observing periods (Stern and Ploshay 1987). A preliminary experiment was performed using this revised version and the results were quite favorable in the track forecast of David compared to that using ECMWF FGGE IIIB. This improvement may be for many reasons including model resolution and data assimilation method.

3. Summary

The numerical results indicate that degradation of skill in predicting track and intensification of tropical storms occurs when going from simulation mode (specification of lateral boundary conditions from an observational analysis) to forecast mode (specification of lateral boundaries from a global forecast). For accurately predicting storm genesis there exists a need for a better forecast of the large scale environment, a better treatment of the lateral boundary of the regional model, and, depending on the forecast period, an extended domain size of the regional model. It appears that the forecast of tropical cyclones needs a high level of accuracy of the initial data. Two separate large scale analyses resulted in dramatically different results. Perhaps a regional analysis using more data in the vicinity of the disturbance would increase both the quality of the initial analysis and the prediction.

REFERENCES

Akima, H., 1978: A method of bivariate interpolation and smooth surface fitting for irregularly distributed data points. *ACM Trans. Math. Software,* **4**(2), 148–159.

Bengtsson, L., H. Bottger and M. Kanamitsu, 1982: Simulation of hurricane-type vorticies in a general circulation model. *Tellus,* **34,** 440–457.

Bjorheim, K., P. Julian, M. Kanamitsu, P. Kallberg, P. Price, S. Price, S. Tracton and S. Uppsala, 1981: FGGE IIIB daily global analysis. Parts 1–4. European Centre for Median Range Weather Forecasts, [Available from ECMWF, Shinfield Park, Reading, Berkshire RG2 9AX, United Kingdom.]

Ceselski, B. F., 1974: Cumulus convection in weak and strong tropical disturbances. *J. Atmos. Sci.,* **31,** 1241–1255.

Chang, S. W. and R. V. Madala, 1980: Numerical simulation of the influence of sea surface temperature on translating tropical cyclones. *J. Atmos. Sci.,* **37,** 2617–2630.

Charney, J. G. and A. Eliassen, 1964: On the growth of the hurricane depression. *J. Atmos. Sci.,* **21,** 68–75.

Digon, N. E., 1987: Formation of Hurricane Frederic 1979: Numerical experiment. *17th Conf. on Hurricanes and Tropical Meteorology.* Amer. Meteor. Soc., 312–315.

Frank, N. L. and G. Clark, 1980: Atlantic tropical systems of 1979. *Mon. Wea. Rev.,* **108,** 966–972.

Gordon, C. T. and W. F. Stern, 1982: A description of the GFDL global spectral model. *Mon. Wea. Rev.,* **110,** 625–644.

Gray, W.M., 1968: Global view of the origin of tropical disturbances and storms. *Mon. Wea. Rev.,* **96,** 669–700.

Hack, J. J. and W. H. Schubert, 1986: Nonlinear response of atmospheric vorticies to heating by organized cumulus convection. *J. Atmos. Sci.,* **43,** 1559–1573.

Hebert, P. J., 1978: Intensification criteria for tropical depressions of the western North Atlantic. *Mon. Wea. Rev.,* **106,** 831–840.

Krishnamurti, T. N., R. J. Pasch, H. Pan, S. Chu and K. Ingles, 1983: Details of low latitude medium range numerical weather prediction using a global spectral model I: Formation of a monsoon depression. *J. Meteor. Soc. Japan,* **61,** 188–206.

——, K. Ingles, S. Cocke, T. Kitade and R. Pasch, 1984: Details of low latitude medium range numerical weather prediction using a global spectral model II: Effects of Orography and Physical Initialization. *J. Meteor. Soc. Japan,* **62,** 613–649.

Kurihara, Y.,1973: A scheme of moist convective adjustment. *Mon. Wea. Rev.,* **101,** 547–553.

—— and M. A. Bender, 1980: Use of a movable nested-mesh model for tracking a small vortex. *Mon. Wea. Rev.,* **108,** 1792–1809.

—— and R. E. Tuleya, 1981: A numerical simulation study on the genesis of a tropical storm. *Mon. Wea. Rev.,* **109,** 1629–1653.

—— and M. A. Bender, 1983: A numerical scheme to treat the open lateral boundary of a limited area model. *Mon. Wea. Rev.,* **111,** 445–454.

Lee, C. S., 1986: Large scale circulation pattern associated with tropical cyclone formation during FGGE year. *Nat. Conf. on Scientific Results of the FGGE.* Amer. Meteor. Soc., 208–211.

McBride, J. L. and R. Zehr, 1981: Observational analysis of tropical cyclone formation. Part II: Comparison of non-developing versus developing systems. *J. Atmos. Sci.,* **38,** 1132–1151.

Manabe, S., J. L. Holloway and H. M. Stone, 1970: Tropical circulation in a time-integration of a global model of the atmosphere. *J. Atmos. Sci.,* **27,** 580–613.

Mellor, G. L. and T. Yamada, 1974: A hierarchy of turbulence closure models for planetary boundary layers. *J. Atmos. Sci.,* **31,** 1791–1806.

Miller, B. I., P. P. Chase and B. R. Jarvinen, 1972: Numerical prediction of tropical weather systems. *Mon. Wea. Rev.*, **100,** 825–835.

Miyakoda, K., J. Sheldon and J. Sirutis, 1982: Four-dimensional analysis experiment with the GATE data. Part II. *J. Atmos. Sci.*, **39,** 486–506.

Ooyama, K. V., 1964: A dynamic model for the study of tropical cyclone development. *Geofys. Init.*, **4,** 187–198.

——, 1982: Conceptual evaluation of the theory and modeling of the tropical cyclone. *J. Meteor. Soc. Japan,* **60,** 369–380.

Orlanski, I. and J. J. Katzfey, 1987: Sensitivity of model simulations for a coastal cyclone. *Mon. Wea. Rev.*, in press.

Ploshay, J. J., R. White and K. Miyakoda, 1983: FGGE Level IIIB daily global analysis, Parts 1–4. Dec. 1978–Nov. 1979. *NOAA Data Report,* ERL/GFDL-1, 278 pp. [Available from GFDL, Box 308, Princeton, NJ 08542.]

Rotunno, R. and K. A. Emanuel, 1987: An air–sea interaction theory for tropical cyclones. Part 2: Evolutionary study using a nonhydrostatic axisymmetric numerical model. *J. Atmos. Sci.*, **44,** 542–561.

Sadler, J. C., 1978: Mid-season typhoon development and intensity changes and the tropical upper tropospheric trough. *Mon. Wea. Rev.*, **106,** 1137–1152.

Shapiro, L. J., 1977: Tropical storm formation from easterly waves: A criterion for development. *J. Atmos. Sci.*, **34,** 1007–1021.

Shea, D. J. and W. M. Gray, 1973: The hurricane's inner core region. I: Symmetric and asymmetric structure. *J. Atmos. Sci.*, **30,** 1544–1564.

Smagorinsky, J., 1963: General circulation experiments with the primitive equations: I. The basic experiment. *Mon. Wea. Rev.*, **91,** 99–164.

Stern, W. F. and J. J. Ploshay, 1987: The post-FGGE data assimilation system at GFDL. *Global Weather Experiment Newsletter,* **17,** 5–13. BASC, JH810, National Academy of Sciences/NRC, 2101 Constitution Ave., NW, Washington, D.C. 20418

——, —— and K. Miyakoda, 1985: Continuous data assimilation at GFDL during FGGE. *Report at Seminar/Workshop 1984 on data systems and observing system experiments with particular emphasis on FGGE.* Vol. 2, ECMWF and WMO, 157–190.

Tuleya, R. E. and Y. Kurihara., 1981: A numerical study on the effects of environmental flow on tropical storm genesis. *Mon. Wea. Rev.*, **109,** 2487–2506.

—— and ——, 1982: A note on the sea surface temperature sensitivity of a numerical model of tropical storm genesis. *Mon. Wea. Rev.*, **110,** 2063–2069.

—— and ——, 1984: The formation of comma vortices in a tropical numerical simulation model. *Mon. Wea. Rev.*, **112,** 491–502.

——, M. A. Bender and Y. Kurihara, 1984: A simulation study of the landfall of tropical cyclones using a movable nested-mesh model. *Mon. Wea. Rev.*, **112,** 124–136.

Wendland, W. M., 1977: Tropical storm frequencies related to sea surface temperatures. *J. App. Meteor.*, **16,** 477–481.

Wetherald, R. T. and S. Manabe, 1980: Cloud cover and climate sensitivity. *J. Atmos. Sci.*, **37,** 1485–1510.

Willoughby, H. E., F. D. Marks, Jr. and R. J. Feinberg, 1984: Stationary and moving convective bands in hurricanes. *J. Atmos. Sci.*, **41,** 3189–3211.

Yanai, M., 1961a: A detailed analysis of typhoon formation. *J. Meteor. Soc. Japan,* **39,** 187–214.

——, 1961b: Dynamical aspects of typhoon formation. *J. Meteor. Soc. Japan,* **39,** 282–309.

——, 1968: Evolution of a tropical disturbance in the Caribbean Sea region. *J. Meteor. Soc. Japan,* **46,** 86–109.